



HHS Public Access

Author manuscript

J Med Chem. Author manuscript; available in PMC 2024 July 13.

Published in final edited form as:

J Med Chem. 2023 July 13; 66(13): 9076–9094. doi:10.1021/acs.jmedchem.3c00664.

Alicyclic Ring Size Variation of 4-Phenyl-2-naphthoic Acid Derivatives as P2Y₁₄ Receptor Antagonists

Zhiwei Wen,

Molecular Recognition Section, Laboratory of Bioorganic Chemistry, National Institute of Diabetes and Digestive and Kidney Diseases, National Institutes of Health, Bethesda, Maryland 20892, United States

Asmita Pramanik,

Molecular Recognition Section, Laboratory of Bioorganic Chemistry, National Institute of Diabetes and Digestive and Kidney Diseases, National Institutes of Health, Bethesda, Maryland 20892, United States

Sarah A. Lewicki,

Molecular Recognition Section, Laboratory of Bioorganic Chemistry, National Institute of Diabetes and Digestive and Kidney Diseases, National Institutes of Health, Bethesda, Maryland 20892, United States

Young-Hwan Jung,

Molecular Recognition Section, Laboratory of Bioorganic Chemistry, National Institute of Diabetes and Digestive and Kidney Diseases, National Institutes of Health, Bethesda, Maryland 20892, United States

Zhan-Guo Gao,

Molecular Recognition Section, Laboratory of Bioorganic Chemistry, National Institute of Diabetes and Digestive and Kidney Diseases, National Institutes of Health, Bethesda, Maryland 20892, United States

John C. R. Randle,

Random Walk Ventures, LLC, Boston, Massachusetts 02111, United States

Chunxia Cronin,

Pat and Jim Calhoun Cardiology Center, University of Connecticut Health Center, Farmington, Connecticut 06030, United States

Zhoumou Chen,

Corresponding Author: Kenneth A. Jacobson – Molecular Recognition Section, Laboratory of Bioorganic Chemistry, National Institute of Diabetes and Digestive and Kidney Diseases, National Institutes of Health, Bethesda, Maryland 20892, United States; Phone: 301-496-9024; kennethj@nidk.nih.gov; Fax: 301-496-9024.

Supporting Information

The Supporting Information is available free of charge at <https://pubs.acs.org/doi/10.1021/acs.jmedchem.3c00664>.

Schemes S1 and S2 and synthetic methods, additional binding data, determination of lipophilicity by HPLC, off-target activities, ADMET properties, results from asthma, chronic pain, cardiac ischemia models, NMR spectra and HPLC purity, and calculated ADMET properties (PDF)

Molecular strings P2Y₁₄ (CSV)

Complete contact information is available at: <https://pubs.acs.org/doi/10.1021/acs.jmedchem.3c00664>

The authors declare no competing financial interest.

Department of Pharmacology and Physiology and the Henry and Amelia Nasrallah Center for Neuroscience, Saint Louis University School of Medicine, St. Louis, Missouri 63104, United States

Luigino A. Giancotti,

Department of Pharmacology and Physiology and the Henry and Amelia Nasrallah Center for Neuroscience, Saint Louis University School of Medicine, St. Louis, Missouri 63104, United States

Gregory S. Whitehead,

Immunity, Inflammation and Disease Laboratory, National Institute of Environmental Health Sciences, National Institutes of Health, Research Triangle Park, North Carolina 27709, United States

Bruce T. Liang,

Pat and Jim Calhoun Cardiology Center, University of Connecticut Health Center, Farmington, Connecticut 06030, United States

Sylvie Breton,

Centre de Recherche du CHU de Québec, Département d'Obstétrique, de Gynécologie et Reproduction, Faculté de Médecine, Université Laval, Laval, Québec G1V 4G2, Canada

Daniela Salvemini,

Department of Pharmacology and Physiology and the Henry and Amelia Nasrallah Center for Neuroscience, Saint Louis University School of Medicine, St. Louis, Missouri 63104, United States

Donald N. Cook,

Immunity, Inflammation and Disease Laboratory, National Institute of Environmental Health Sciences, National Institutes of Health, Research Triangle Park, North Carolina 27709, United States

Kenneth A. Jacobson

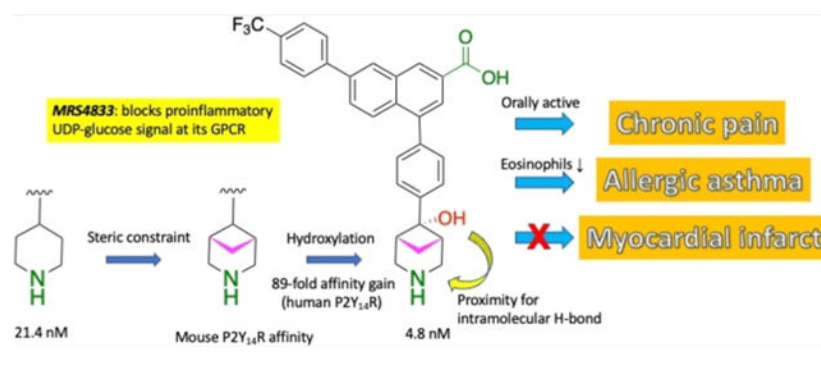
Molecular Recognition Section, Laboratory of Bioorganic Chemistry, National Institute of Diabetes and Digestive and Kidney Diseases, National Institutes of Health, Bethesda, Maryland 20892, United States

Abstract

P2Y₁₄ receptor (P2Y₁₄R) is activated by extracellular UDP-glucose, a damage-associated molecular pattern that promotes inflammation in the kidney, lung, fat tissue, and elsewhere. Thus, selective P2Y₁₄R antagonists are potentially useful for inflammatory and metabolic diseases. The piperidine ring size of potent, competitive P2Y₁₄R antagonist (4-phenyl-2-naphthoic acid derivative) PPTN **1** was varied from 4- to 8-membered rings, with bridging/functional substitution. Conformationally and sterically modified isosteres included *N*-containing spirocyclic (**6–9**), fused (**11–13**), and bridged (**14, 15**) or large (**16–20**) ring systems, either saturated or containing alkene or hydroxy/methoxy groups. The alicyclic amines displayed structural preference. An α -hydroxyl group increased the affinity of 4-(4-((1*R*,5*S*,6*r*)-6-hydroxy-3-azabicyclo[3.1.1]heptan-6-yl)phenyl)-7-(4-(trifluoromethyl)-phenyl)-2-naphthoic acid **15** (MRS4833) compared to **14** by 89-fold. **15** but not its double prodrug **50** reduced airway eosinophilia in a protease-mediated

asthma model, and orally administered **15** and prodrugs reversed chronic neuropathic pain (mouse CCI model). Thus, we identified novel drug leads having in vivo efficacy.

Graphical Abstract



INTRODUCTION

Activation of the G_i protein-coupled P2Y₁₄ receptor (P2Y₁₄R, previously designated GPR105) is proinflammatory in various cell types, and its principal native full agonist UDP-glucose (UDPG) is considered a damage-associated molecular pattern (DAMP).^{1–5} In classically activated M1 macrophages, the endogenous P2Y₁₄R agonist UDPG results in transcription factor STAT1 activation, which induces the expression of proinflammatory mediators.¹ In mouse epithelial cells, the receptor activates the production and secretion of interleukin-8 (IL-8) murine homologues (i.e., CXCL1 and CXCL2) following renal ischemia-reperfusion injury, which was attenuated with a P2Y₁₄R antagonist. A marked elevation of IL-1 β was almost completely abolished by the P2Y₁₄R antagonist.^{2–4} The renal P2Y₁₄R in collecting duct intercalated cells mediates chemokine expression, followed by neutrophil and monocyte infiltration. These neutrophils and monocytes “attack” proximal tubule cells that were weakened by ischemia and induce proximal tubule damage.⁴ In a protease-induced asthma model, P2Y₁₄R activation on eosinophils increases their chemokinesis, resulting in the passage of eosinophils from the blood to the lungs and increased airway inflammation, which is reduced by antagonists.⁶

Selective P2Y₁₄R antagonists are desired for their anti-inflammatory effect, given the proinflammatory activity of UDPG. Other UDP-sugars, i.e., UDP-galactose, UDP-glucuronic acid, UDP-*N*-acetylgalactosamine, and UDP-*N*-acetylglucosamine activated P2Y₁₄R with lower potency,⁷ and UDP has been characterized as a potent partial agonist.⁸ Thus, P2Y₁₄R antagonists could potentially be useful for the treatment of inflammation, kidney disease, asthma, diabetes, obesity, chronic pain, gout, and neurofibromatosis.^{6,9–13} On the other hand, P2Y₁₄R activation in autologous cardiac progenitor cell therapy might benefit heart failure.¹⁴ An important pharmacological tool molecule for this receptor is the selective antagonist 4-phenyl-2-naphthoic acid derivative **1** (PPTN, Chart 1), originally identified in a patent by Belley et al.¹⁵ Compound **1** was shown by Harden and colleagues to bind selectively to the P2Y₁₄R as a high-affinity antagonist with a *K_i* value of 0.43 nM in reversing agonist-induced inhibition of cAMP production.¹⁶ We later introduced a

fluorescent binding assay that is suitable for routine drug screening at the P2Y₁₄R, and **1** displayed IC₅₀ values of 6–8 nM in a whole-cell fluorimetric assay.^{5,17}

We are exploring the structure–activity relationship (SAR) of 4-phenyl-2-naphthoic acid derivatives related to **1** as P2Y₁₄R antagonists, both as pharmacological tool molecules and as potential translational compounds. Previous publications have focused on all regions of the zwitterionic **1** scaffold and have identified both charged and uncharged bioisosteres.^{5,17} Human (h) P2Y₁₄R structural modeling based on the X-ray crystallo-graphic structure of the closely homologous ADP-responsive P2Y₁₂R has aided in the selection of target molecules to synthesize based on their predicted binding to the P2Y₁₄R orthosteric site.^{5,17} However, **1** is amphiphilic and has low oral bioavailability (5% F, in mouse).¹⁸ To address this short-coming, orally active prodrugs of **1** and its recently introduced analogues have been successfully identified using an *N,N*-dimethylamidomethyl esterification of the important naphthalene-carboxylic acid moiety.^{5,18,19}

Recent SAR studies have focused on the modification or replacement of the piperidine moiety of **1**, which is predicted to point outward from the P2Y₁₄R orthosteric binding site.^{5,10,17} We have utilized that insight to make chain extensions from the piperidine N that still retain receptor affinity and in vivo efficacy in pain and asthma models. Charged amino derivatives, e.g., **2a** and **2b** and an uncharged isoxazole **3**, were found to contain suitable isosteric replacements for the piperidine ring. Among the many charged derivatives we reported, quinclidine **2a** and (1*S*,4*S*,5*S*)-5-phenyl-2-azabicyclo[2.2.1]heptane (a 2-azanorbornane) **2b** derivatives displayed notably high affinity.^{5,17} Thus, constraining the piperidine ring of **1** in a receptor-preferred conformation was a productive means of increasing three-dimensionality and at the same time preserving or enhancing binding affinity. Other chemotypes have been reported to be P2Y₁₄R antagonists, including the 2-phenyl-benzoxazole acetamide derivative **4a** and 5-amide-1*H*-pyrazole-3-carboxyl derivative **4b**.^{20,21}

Here, we have varied the ring size of the alicyclic amine of **1** from four to eight atoms, with bridging and functional group substitution, including spiro and fused cyclo(aza)aliphatic rings. The occurrence, conformation, and utility of various cycloalkyl rings in experimental drugs have been reviewed.^{22–24} These new derivatives complement our recent study of analogues in which the piperidine moiety has been sterically constrained with one- and two-carbon bridges.⁵ Surprisingly, not only were prodrug derivatives protective in a chronic pain model (either mono-ester or mixed ester/carbamate double prodrugs), but a potent, sterically constrained zwitterionic parent drug **15** (with mP2Y₁₄R affinity 4.5-fold higher affinity than reference antagonist **1**) was highly efficacious upon oral administration.

RESULTS AND DISCUSSION

Selection of Compounds Prepared.

In an effort to explore other scaffolds reported to be P2Y₁₄R antagonists as potential lead compounds, in addition to the piperidine series of **1**, we considered recently reported antagonists **4a** (Zhou et al.) and **4b** (Wang et al.).^{20,21} We resynthesized the uncharged, small molecular P2Y₁₄R antagonist **4a** in the 2-phenyl-benzoxazole acetamide series

(Scheme S1, Supporting information, compound **46** in Zhou et al.²⁰). We evaluated the compound in a whole cell (hP2Y₁₄R-expressing CHO cells) binding assay using **52** (Supporting Information), a fluorescent analogue of **1** used in our previous studies.⁵ However, no binding inhibition by **4a** was observed up to 100 μ M, indicating a lack of binding to the receptor orthosteric site (Table S1, Figure S1, Supporting Information). Therefore, it was not a suitable lead for further derivatization as a competitive antagonist. We did not perform a cAMP assay of **4a** or test the possibility of allosteric receptor modulation.

We then returned our attention to the 4-phenyl-2-naphthoic acid series related to **1** and continued the SAR exploration of this high-affinity series.^{5,17} There is considerable steric and conformational freedom to vary the piperidine moiety, as noted earlier. By varying the ring size and introducing bridging and fused rings as well as functional groups (Table 1), we aimed to identify antagonists with nM affinity at the P2Y₁₄R. Although we recently reported many bicyclic variations of piperidine within this chemical series and identified (*S,S,S*)-2-azanorbornane derivative **2b** as a particularly potent P2Y₁₄R antagonist, there were additional potential bioisosteres of piperidine that could be compared.

Chemical Synthesis.

The preferred synthesis of P2Y₁₄R antagonists based on **1** as a lead includes, sequentially, a Grignard reaction of a ketone-containing starting material for the generation of a bromophenyl intermediate, a Suzuki coupling of the bromophenyl intermediate, such as **21** (Scheme 1), with boronic acid pinacol ester **22** to obtain the 4-phenyl-2-naphthoic acid core structure, ester hydrolysis to a free carboxylic acid, Boc/benzyl deprotection to a free amine, and conversion of some of the analogues obtained to their related ligands. Thus, the smallest ring analogue, i.e., azetidine analogue **5**, was prepared via Suzuki coupling between commercially available 3-(4-bromophenyl)azetidine **21**, without *N*-protection, and a naphthalenyl boronic acid pinacol ester **22**⁴¹ followed by ester hydrolysis. A small-scale hydrolysis reaction (6 mg of **23**) was performed followed by HPLC purification, which gave a relatively low yield of 47%.

The preparation of analogues of **1** with piperidine substitutions consisting of 2-azaspiro[3.3]heptane (Scheme 2A), octahydrocyclopenta[*c*]pyrrole (B), 3-azabicyclo[3.1.1]heptane (C), 1-azacycloheptane (D), and azocane (E) are summarized in Scheme 2. In a one-pot reaction, treatment of ketones **24**, **28**, **32**, **36**, and **40** with in situ generated Grignard reagent 4-bromophenylmagnesium bromide provided bromophenyl intermediates **25**, **29**, **33**, **37**, and **41**, respectively. Derived from a racemic starting material **28**, intermediate **29** is a racemic mixture of left-handed and right-handed helical enantiomers. A stereoselective Grignard reaction of **32** yielded enantiomer **33** with a hydroxyl group and one-carbon bridge identified as *trans* to each other.

The Suzuki coupling of naphthalenyl boronic acid pinacol ester **22** with the 4-(4-bromophenyl) intermediates **25**, **29**, **33**, **37**, and **41** gave their corresponding esters of analogues **26**, **30**, **34**, **38**, and **42**, respectively. The ester hydrolysis of **26**, **30**, **34**, **38**, and **42** provided the derivatives **27**, **31**, **35**, **39**, and **43**, respectively. Boc deprotection of **27** with TFA in

DCM offered product **8** in addition to dehydrated product **7**. Compound **8** was unstable in the reaction residue in the presence of methanol and partially reacted with methanol and methanol- d_4 to give *O*-methylated ligand **9**, and its isotopic ratio was estimated by NMR. Thus, methanol should be avoided if a methylated by-product is not needed. Similarly, Boc deprotection of **43** gave product **20** and dehydrated compound **19**. Nevertheless, Boc deprotection of **39** meanwhile dehydrated the hydroxyl group to yield alkene mixture **17**. Boc deprotection of compound **35** simply gave α -hydroxyl-3-azabicyclo[3.1.1]heptan-6-yl derivative **15**. Pd-catalyzed debenzylation of **31** with H_2 afforded ligand **11**, which was further dehydrated by refluxing in TFA to give **12**. Reduction of **7**, **12**, and **17** by Pd-catalyzed hydrogenation offered analogues of **1**, i.e., **6** with 2-azaspiro[3.3]heptane (Scheme 2A), **13** with octahydrocyclopenta[*c*]pyrrole (B), and **16** with 1-azacycloheptane (D), respectively. Stereoselective deoxygenation⁵ of **15** with sodium borohydride in sulfuric acid afforded **14**. Thus, hygroscopic sulfuric acid was employed to readily generate a tertiary benzylic carbocation, which was further reduced by sodium borohydride to yield deoxygenated product.

Compound **18** would be obtained from **19** via hydrogenation using hydrogen gas (condition e, Scheme 2). Nevertheless, the preparation of **19** from dehydration of **43** in TFA/DCM (Scheme 2E) suffered from a low yield. Thus, an alternative synthetic strategy was developed as shown in Scheme 3. Dehydration²⁷ of 5-hydroxylazocane **41** using triphosgene and 4-dimethylaminopyridine (DMAP) under mild conditions gave alkene **44** in a quantitative yield. The Suzuki coupling of **22** with **44** gave ester **45**. Reduction catalyzed by Pd/C²⁸ of **45** was carried out using triethylsilane as the hydrogen source, in which hydrogen was generated and used for reduction in situ. Boc deprotection of **46** followed by ester hydrolysis provided the azocane analogue **18** with an overall yield of 54% from **45** after three reaction steps (steps c, d, and e), during which crude residues from steps c and d were used directly for the next steps without column purification.

Our previous study⁵ demonstrated unanticipated potent in vivo activity in a mouse asthma model of single (ester or carbamate²⁹) and double prodrugs of **2b**. Also, a *N,N*-dimethylamidomethyl ester prodrug of **1** was previously shown to be orally bioavailable.¹⁸ Using an analogous strategy to prepare prodrugs of potent antagonist **15**, a *N,N*-dimethylamidomethyl ester prodrug **49** was prepared in two steps from the amino-protected parent carboxylic acid **35** via esterification using 2-chloro-*N,N*-dimethylacetamide in the presence of base Cs_2CO_3 to give **48** (Scheme 4). The Boc deprotection of **48** gave ester prodrug **49**. The reaction of **49** with ethyl chloroformate provided the double prodrug **50** bearing both ester and carbamate moieties. The carbamate prodrug **51** was synthesized from the treatment of the parent drug **15** with ethyl chloroformate. Table 1 also lists, for comparison, the corresponding double prodrug (ester/carbamate) of **1**, i.e., compound **62**, and two previously reported prodrugs of **2b**, i.e., **63** and **64**.

Absorption, distribution, metabolism, excretion, and toxicity (ADMET) properties were calculated using the StarDrop software (Tables 1 and S6, Supporting Information).²⁵ Most compounds were predicted to be excluded from crossing the BBB, but active drugs **2a**, **7**, **12**, **17**, and **19**, and prodrug **49** had profiles consistent with some bioavailability in the brain

(19% of blood level). All of these active drugs, except **19**, were of relatively high affinity ($IC_{50} > 20$ nM) at the hP2Y₁₄R. Compounds **5–8** and **10–20** each had only 5 rotatable bonds with MW ~500. Key antagonist **15** had Log *D* of 2.37, TPSA of 70 Å², 3 H-bond donors, 4 H-bond acceptors, and ligand efficiency (LE) of 0.311, which is within a drug-like range.⁴⁹

Pharmacological Evaluation.

The synthesized analogues were compared in hP2Y₁₄R affinity in a fluorescent whole-cell competitive binding assay, by measuring displacement by flow cytometry using the antagonist fluorescent tracer **52** (20 nM), which contains an AlexaFluor488 fluorophore (Figure 1).³⁰ Although a sub-nanomolar hP2Y₁₄R affinity of **52** was previously determined in a cAMP assay,³⁰ we reexamined its affinity in a fluorescent binding saturation study in whole CHO cells expressing the hP2Y₁₄R. A K_D value of 27.8 ± 9.3 nM ($n = 5$) was determined as shown in Figure 1. This K_D value allowed using the Cheng-Prusoff equation³¹ to convert the IC_{50} values to K_i values, which we report here for both the newly prepared compounds and those from our previous SAR studies⁵ of this chemical series (Table 1). Except for monoester **49** and monocarbamate **51**, most of the mono and double prodrugs were not measured in the binding assays, because previous experience indicates very low P2Y₁₄R affinity for similar derivatives lacking a free carboxylate.³⁰

We have used a bitopic fluorescent probe compound **52** as the basis of our receptor binding assay. In an effort to improve our in vitro assay, we attached a novel tricyclic fluorophore (JaneliaFluor 646) that has advantages for protein labeling³² to an amino-functionalized intermediate, i.e., **58**, used previously to prepare **52** (Scheme S2, Supporting Information). However, this new fluorescent conjugate **53** did not demonstrate potent specific binding in whole CHO cells expressing the hP2Y₁₄R under the similar conditions used for **52** within a range of final concentrations of **53** of 2, 100, 500, and 20,000 nM (Supporting Information) compared to a concentration of **52** of 20 nM. This surprising result emphasized that distal functional groups on the fluorophore coupled to the antagonist pharmacophore can have a major effect on the receptor interactions.

A piperidine moiety is commonly found in a wide range of pharmaceuticals and natural products.³³ Systematic approaches to identify piperidine bioisosteres and bridged piperidines as phenyl bioisosteres have been reported for diverse targets^{34,35} and for P2Y₁₄R antagonists.⁵ We have substituted the piperidine moiety of **1** with nitrogen-containing spirocyclic (**6–9**), fused (**11–13**), and bridged (**14, 15**) or large (**16–20**) ring systems, either fully saturated or containing one alkene or hydroxy/methoxy group. The P2Y₁₄R affinity varied considerably, from IC_{50} 5.9 nM (**15**) to >500 nM, indicating that although this moiety binds in a relatively flexible receptor region as predicted in earlier modeling,⁵ there is still a steric and conformational preference for this moiety.

Four-membered and spiro ring substitution has been applied widely in medicinal chemistry.³⁶ In the current series such substitution in **5–9** led to intermediate P2Y₁₄R affinity, except for unsaturated analogue **7**, which displayed an IC_{50} of 9.69 nM. The highest affinity among five-membered ring analogues was with racemic fused 5-hydroxyoctahydrocyclopenta[*c*]-pyrrol-5-yl derivative **11**, with an IC_{50} of 9.48 nM.

An 2-azaspiro[3.3]heptane analogue was only moderately potent in P2Y₁₄R binding, but its affinity was enhanced 4.8-fold upon introduction of unsaturation in **7**. 2-Azaspiro[3.3]heptane was previously identified as a piperidine bioisostere.³⁷ However, it is to be noted that the success of a given bioisostere is target-dependent due to the constraints of each binding environment.

Given the high affinity of piperidine derivative **1** and its bicyclic analogues **2a** and **2b**,^{5,17} we introduced a fused four-membered ring on the piperidine ring of **1** in **14** and **15**. This variation on a six-membered ring substituent displayed high affinity, only in the case of (1*R*,5*S*,6*r*)-6-aryl-3-azabicyclo-[3.1.1]heptan-6-ol derivative **15** (IC₅₀ 5.92 nM), containing a α -hydroxyl group trans to the carbon bridge. The seven-membered ring analogues **16** and **17** also displayed relatively high affinity with IC₅₀ values of ~10 nM at the P2Y₁₄R. The benefits and conformational properties of seven-membered rings in medicinal chemistry have recently been reviewed.³⁸ However, the eight-membered ring analogues **18–20** were found to have the lowest affinity among these derivatives (Table 1).

Selected compounds were additionally evaluated in binding to the mouse (m) P2Y₁₄R expressed in HEK-293 cells (Table 2) using a whole-cell fluorescent binding assay with fluorescent tracer **52**. Five out of the nine analogues compared at the two species had IC₅₀ values within a factor of 2. Potent reference antagonist **2b** was 11-fold weaker at the mP2Y₁₄R, while racemic (3*aR*,6*aR*)-1,2,3,3*a*,4,6*a*-hexahydrocyclopenta[*c*]-pyrrol-5-yl derivative **12** was 3-fold more potent at the mP2Y₁₄R.

The starkest contrast of two closely related alicyclic amines substituted for the piperidine moiety of **1**, among both α -hydroxy and non- α -hydroxy analogues, was seen with the 3-azabicyclo[3.1.1]heptan-6-yl system in **14** and **15**. The presence of an α -hydroxyl group increased the affinity by roughly 100-fold. However, there was only a small effect of a hydroxyl group in **B** compared to piperidine analogue **A** (compound **1**, Table 1). In our previous study (Table 3),⁵ a hydroxyl group present on the piperidine ring α -carbon fused to the phenyl ring had variable effects. In the case of nortropine derivative **C** (IC₅₀ 38.3 ± 2.0 nM), a hydroxyl group in **D**, *cis*-oriented with respect to the ethylene bridge, reduced affinity (IC₅₀ 117 ± 38 nM). However, a hydroxyl group (reversed stereochemistry) greatly increased the P2Y₁₄R affinity of **F** (IC₅₀ 21.3 ± 1.1 nM) compared to **E** (IC₅₀ 696 ± 100 nM).

Off-target radioligand binding activity of five analogues (**7**, **11**, and **15–17**) at diverse receptors was examined by the NIMH Psychoactive Drug Screening Program (PDSP). Weak μ M interactions were found, reflecting the relative selectivity of these antagonists for their target receptor (Supporting Information).³⁹ Binding (K_i , μ M) to the σ_1 receptor (**16**, 0.89; **17**, 0.84) and σ_2 receptor (**7**, 2.2; **16**, 2.8; **17**, 3.9) was observed for several analogues. Additional interactions were observed at the serotonin 5-HT_{1B} (**7**, 6.7; **11**, 5.4; **15**, 6.0; **16**, 4.5; **17**, 4.1), 5-HT_{5A} (**11**, 2.4; **16**, 4.8; **17**, 4.0), muscarinic M₅ (**7**, 5.0; **15**, 6.0), histamine H₁ (**7**, 5.6; **16**, 2.8), adrenergic β_3 (**7**, 6.8; **16**, 6.6; **17**, 6.3), α_{1B} (**7**, 7.3; **11**, 6.4; **17**, 7.4), α_{2A} (**11**, 5.7) and κ -opioid (**17**, 0.46) receptors.

The ligands' lipophilicities were determined based on their HPLC retention time in comparison to known compounds.^{5,40} Using the five standard compounds with reported distribution coefficient $\text{Log } D_{7.4}$ (Table S2, Supporting Information), a calibration line of $\text{Log } D_{7.4}$ vs retention factor k (Figure S3) was plotted for calculating HPLC-based $\text{Log } D_{7.4}$ of the analogues. The $\text{Log } D_{7.4}$ values are summarized in Figure S4 and Table 1. The lipophilicities of all of the ligands were consistent with their structures. The lipophilicities of ligands increased as the heterocyclic ring size increased from 4- to 8-membered (from compounds **5**, **10**, **1**, and **16** to **18**). Most of other compounds had higher lipophilicities compared to lead compound **1**, except **8**, **11**, **15**, and **20** that all had a hydroxyl group at the benzyl position of the alicyclic amino substituent. All of these less lipophilic active drugs, except **20**, bound with relatively high hP2Y₁₄R affinity ($\text{IC}_{50} > 20$ nM). However, none of these more polar derivatives were predicted to cross the blood–brain barrier (BBB).

Experimental studies of the absorption, distribution, metabolism, excretion, and toxicity (ADMET) properties of compound **15** were carried out. Both in vitro and in vivo results indicated that the compound was suitable for further testing in animal models of disease (Table S3, Supporting Information). Four doses of **15** (1, 3, and 10 mg/kg, i.p. and 0.5 mg/kg, i.v.) were administered in male Wistar rats and compared to our previous data determined using the same methods for **2b**.⁵ No mortality or morbidity was observed in any of the groups, and all animals were normal throughout the experimental period. Although oral bioavailability was not examined, the drug has a substantial half-life in plasma following i.p. administration (Figure 2). The $t_{1/2}$ values of **2b** and **15** (3 mg/kg) were 8.6 and 4.3 h, respectively. Strikingly, the bioavailability of **2b** and **15** diverged with 43 and 114%F (3 mg/kg, i.p.), respectively. The drug exposure ($\text{AUC}_{0-\text{last}}$) was proportional to the dose for **15** but not for **2b**, and the clearance (Cl) was nearly identical across doses for **15** but not for **2b**. The volume of distribution (V_d) was considerably lower for **15** compared to **2b**, indicating a tendency to remain in the plasma. This parameter was also consistent with its lower lipophilicity ($\text{Log } D_{7.4}$ of 1.2) compared to many of the other analogues, including **2b** ($\text{Log } D_{7.4}$ of 1.9).

Compound **2b** was more stable than **15** in simulated gastric fluid, both were stable in simulated intestinal fluid, and neither compound displayed liver cell toxicity (Table 4). Compounds **2b** and **15** showed IC_{50} values $>30 \mu\text{M}$ for all 5 CYPs tested. The hERG activity was determined separately in a fluorescent assay (method in the Supporting Information), and both compounds showed weak hERG inhibition with $\text{IC}_{50} > 30 \mu\text{M}$. The plasma protein binding of the two antagonists was high in three species.

The pharmacokinetic behavior of reference prodrugs **62** and **63** was characterized in mouse indicating modest oral bioavailability of **62** (Table S5, Supporting Information) and rapid cleavage of the ester group of **63**. The in vivo pharmacokinetics of mono-ester prodrug **63**, administered subcutaneously (10 mg/kg, s.c.) in female CD1 mice was studied (Table S4, Supporting Information). The product (active drug) was the 2-azanorbornyl derivative **2b**, and the conversion in vivo to **2b** was so rapid that the rate of loss of **63** could not be followed. **2b** reached a peak concentration ($\sim 2 \mu\text{g/mL}$) between 2 and 4 h, with a $t_{1/2}$ of 2.63 h. The AUC_{inf} value was 15,300 ng/mL·h. The total amount of **2b** excreted in the

urine was 1550 ng. For comparison with **63**, the corresponding mono-ester of active drug **1** was studied for plasma stability in vitro. Both **63** and the mono-ester of **1** were rapidly hydrolyzed in mouse plasma ($t_{1/2} \sim 1.5$ min), but not human plasma ($t_{1/2} > 720$ min). In a separate study, the in vivo pharmacokinetics of double prodrug **62** (containing both ester and carbamate prodrug moieties) was determined following administration by oral gavage (p.o.) in female CD1 mice (Table S5, Supporting Information). The resulting active drug was compound **1**, and in this case both the prodrug and active drug were detectable, and an in vivo time course was established for the conversion. **62** reached a peak concentration (~ 2 $\mu\text{g/mL}$) at 1 h, with a $t_{1/2}$ of 1.45 h (6.9% F), and **1** reached a peak concentration at 7 h, with a C_{max} of 33 ng/mL. The AUC_{inf} values were 1780 ng/mL*h for **62** and 515 ng/mL*h for **1**. The species dependence of $t_{1/2}$ values and the complexity of the 2-step unmasking of **62** suggest that additional pharmacokinetic studies of the various prodrugs will be needed.

Several antagonists, potent active drugs **11**, **15**, and **16**, mono-ester prodrug **63** and double prodrugs **50**, **62**, and **64**, were subjected to an in vivo mouse model of chronic neuropathic pain (chronic constriction injury, CCI),⁴¹ as applied previously to various P2Y₁₄R antagonists in the same chemical series.¹⁰ The reversal of established chronic neuropathic pain by all analogues is shown in Figure 3. Both administration by oral gavage (Figure 3A,B) and by i.p. injection (for prodrugs **62** and **64** (Figure 3C,D); for active drugs **11**, **15**, and **16**, Figure S8, Supporting Information) provided benefit. Compound **15** achieved full reversal of mechano-allodynia within 0.5 h post-injection (i.p.), as well as nearly complete protection at 1 h post oral gavage. A monoester prodrug **63** of previously reported constrained antagonist **2b** was fully efficacious within 1 h post oral gavage. The protection by **11** (i.p.) was maintained over 3 h, although the maximal efficacy was not as complete as for **15**. We then compared **1** and **15** administered by oral gavage in the same CCI experiment (Figure 3E). Both antagonists reached full reversal of mechano-allodynia, but the duration of the protection by **15** was longer than protection by **1**. Therefore, we have shown a more favorable in vivo profile for **15** compared to the original lead compound **1**. Even with a low oral bioavailability of **1** in the mouse, a sufficient concentration of **1** was reached to demonstrate efficacy in the CCI model.

The unexpected oral activity of **15** in the mouse CCI model might be a function of the spatial proximity of its hydroxyl group to the secondary amine, which would effectively reduce the zwitterionic character (Figure S9, Supporting Information). Intramolecular H-bonds have been reported to increase the permeability, including oral bioavailability, of polar compounds.^{42,43} The hydroxyl group H is 2.4–4.1 Å away from the amine N, while H-bond distances are typically 2.7–3.3 Å, suggesting a possible H-bond between the OH and N at the bridged piperidine.

Two compounds, 3-azabicyclo[3.1.1]heptan-6-yl active drug **15** and its double prodrug **50** (Figure 4) were examined in an in vivo mouse model of allergic asthma, which was used previously to demonstrate the efficacy of compounds **1**, **2b** and others to reduce eosinophilic lung inflammation.^{5,6} Compound **15**, but not the prodrug **50**, demonstrated significant protection in this asthma model, with fewer eosinophils in the bronchoalveolar lavage (BAL) fluid. There were no statistically significant reductions of lymphocytes, macrophages, or

neutrophils in the BAL fluid for any of the antagonists (Figure S7, Supporting Information), although there was a trend toward lower lymphocytes with **1** and **15**. The reason for the lack of activity of the double prodrug is not evident, given that the analogous double (ester and carbamate) prodrug of antagonist **2b** was highly efficacious in the same protease model of asthma.⁵

Myocardial infarction (MI) denotes the death of cardiac myocytes due to extended ischemia, leading to the invasion of inflammatory neutrophils and macrophages,⁴⁴ both of which highly express the P2Y₁₄ R.¹ Myocardial reperfusion is the restoration of coronary blood flow after a period of coronary occlusion. Reperfusion has the potential to salvage ischemic myocardium but paradoxically can cause injury. Myocardial ischemia and reperfusion lead to an inflammatory response that causes further damage to viable tissue around the infarct. Acute and chronic immune responses elicited by myocardial ischemia have an important role in the functional deterioration of the heart.

Compound **15** was tested in a model of protection from cardiac ischemia-reperfusion (I/R) injury in the mouse (Figure S10, Supporting Information). **15** was administered at 2 mg/kg/day in a minipump (1 mL/h) prior to 30 min of myocardial ischemia and 48 h of reperfusion in an established mouse model.^{45,46} The results showed similar AAR/TTA (area at risk/total area of left ventricle) of 33.7 and 32.6% in **15**- and vehicle-treated animals, respectively. **15** did not change the infarct size with similar IF/AAR at 31.8% in the drug-treated group ($n = 12$) vs 26.4% in the control group ($n = 12$, $P = 0.124$). Although this antagonist appears to have good potency and plasma concentration in rodents, **15** provided no protection against heart I/R injury in the mouse, raising the possibility of no role for P2Y₁₄R antagonists in this disease model. However, it is possible that different dosing would demonstrate efficacy.

The potential use of P2Y₁₄R antagonists in disease treatment has motivated us to continue the SAR probing of high-affinity naphthalene-based antagonists. There are envisioned applications of such antagonists at peripheral sites, such as the kidney, but their use in the CNS has been underexplored. Although several studies have indicated pain as a viable target to explore, there is a lack of BBB-penetrant antagonists, which will be addressed in future studies. Recently, a putative UDPG vesicular transporter, SLC35D3, has been identified in the brain,⁴⁷ thus reinforcing the need for a broader selection of antagonists.

In conclusion, as an extension of our previous SAR studies, we have synthesized P2Y₁₄R antagonists that are modified with alternative alicyclic and heteroalicyclic substituents in place of the piperidine moiety of the lead antagonist **1**. The rank order of affinity at hP2Y₁₄R (IC₅₀ of 3–19 nM) was: **15** > **11**, **16**, **7** > **17** > **12** > **18**. At mP2Y₁₄R, IC₅₀ values of <12 nM were observed for **11**, **12**, **15**, and **18**. We have seen that in various cases, achieving the highest affinity in a fluorescent whole-cell binding assay requires the presence of an α -hydroxyl group on the alicyclic ring attached to a 1,4-disubstituted phenyl moiety. The structural basis for the preference of certain constrained alicyclic structures can later be explored using computational modeling. Preliminary ADMET studies indicated that 6-hydroxy-3-azabicyclo[3.1.1]heptan-6-yl derivative **15** was well tolerated in vivo in rat, and the exposure of the drug was considerable, which is predictive of potential target

engagement with the receptor. Among the compounds with the highest affinity, protective efficacy was observed in mouse models of chronic disease conditions. We demonstrate favorable in vivo activity of compound **15** and other P2Y₁₄R antagonists in chronic pain and asthma models. Surprisingly, active zwitterionic **15** and **1** were both efficacious in reducing chronic pain when administered orally in the mouse. However, there was no protection by **15** infused post-MI in the mouse on the size of damaged area or cardiac function compared to control. These compounds can be further tested in vivo, such as in kidney inflammation models,⁴⁸ to determine their suitability as candidates for disease treatment.

EXPERIMENTAL SECTION

Chemical Synthesis.

General Information. Materials and Methods.—All chemicals and anhydrous solvents were obtained directly from commercial sources. Bromo (**21**) and ketone (**24**, **28**, **32**, **36**, and **40**) starting materials were purchased from Enamine (Kyiv, Ukraine). All reactions were carried out under an argon atmosphere using anhydrous solvents unless specified otherwise. Room temperature (rt) refers to 25 ± 5 °C. Silica gel precoated with F254 on aluminum plates was used for thin-layer chromatography (TLC). The spots were examined under ultraviolet light at 254 nm and further visualized, where needed, by anisaldehyde or cerium ammonium molybdate stain solution. Column chromatography was performed on silica gel (40–63 μm, 60 Å). ¹H NMR spectra were recorded on a Bruker 400 MHz spectrometer, and ¹³C NMR spectra were recorded on a Bruker 500 MHz spectrometer. NMR spectra for selected compounds are shown in the Supporting Information. Chemical shifts are given in ppm (δ), calibrated to the residual solvent signal peaks of CDCl₃ (7.26 ppm), CD₃OD (3.31 ppm), or DMSO-*d*₆ (2.50 ppm) for ¹H NMR, and CDCl₃ (77.16 ppm) or CD₃OD (49.00 ppm) for ¹³C NMR, with coupling constant (*J*) values reported in Hz. High-resolution mass (HRMS) measurements were performed on a proteomics optimized Q-TOF-2 (Micromass-Waters). The reversed-phase HPLC (RP-HPLC) was performed using Phenomenex Luna 5 μm C18(2)100A, AXIA, 21.2 mm × 250 mm column. Antagonist purity was determined as 95% using Agilent ZORBAX SB-Aq, 5 μm, 4.6 mm × 150 mm column attached to Agilent 1100 HPLC system. The HPLC traces for compounds tested in vivo (**11**, **15**, **16**, **50**, and **62**) are included in the Supporting Information. The peak at around 3.5 min was the solvent peak, while the peak at around 29 min was eluent perturbation signal during the washing stage. **11**, **15**, and **16** had 100% purity. Compounds **50** and **62** had purities of 95 and 99%, respectively. The HPLC traces for compounds **63** and **64** were reported in Wen et al., 2022⁵ while the same batches of samples were used for the in vivo tests in this work.

4-(4-(Piperidin-4-yl)phenyl)-7-(4-(trifluoromethyl)phenyl)-2-naphthoic Acid (1).

—Prepared as reported.²⁶ ¹H NMR (500 MHz, MeOD) δ 8.78–8.74 (m, 1H), 8.43 (d, *J* = 1.9 Hz, 1H), 8.05–7.97 (m, 4H), 7.93 (dd, *J* = 8.9, 2.0 Hz, 1H), 7.82 (d, *J* = 8.1 Hz, 2H), 7.54 (d, *J* = 8.3 Hz, 2H), 7.50 (d, *J* = 8.2 Hz, 2H), 3.62–3.55 (m, 2H), 3.29–3.19 (m, 2H), 3.13–3.03 (m, 1H), 2.26–2.19 (m, 2H), 2.11–1.99 (m, 2H). ¹³C NMR (126 MHz, MeOD) δ 169.65, 145.25, 145.11, 141.55, 139.84, 138.89, 134.93, 134.46, 132.20, 131.39, 129.50, 129.17, 128.91, 128.62, 127.99, 127.79, 127.69, 126.91, 45.70, 40.88, 31.20.

4-(4-((1S,4S,5S)-2-Azabicyclo[2.2.1]heptan-5-yl)phenyl)-7-(4-(trifluoromethyl)phenyl)-2-naphthoic Acid (2b).—Prepared as reported.⁵ ¹H NMR (500 MHz, MeOD) δ 8.76 (t, J = 1.1 Hz, 1H), 8.44 (d, J = 1.9 Hz, 1H), 8.06–7.97 (m, 4H), 7.94 (dd, J = 8.9, 2.0 Hz, 1H), 7.82 (d, J = 8.2 Hz, 2H), 7.57–7.49 (m, 4H), 4.30–4.25 (m, 1H), 3.32–3.28 (m, 4H), 3.00–2.96 (m, 1H), 2.47–2.38 (m, 1H), 2.25–2.16 (m, 1H), 2.13 (d, J = 11.6 Hz, 1H), 1.87–1.80 (m, 1H); ¹³C NMR (126 MHz, MeOD) δ 169.72, 145.26, 144.53, 141.46, 139.53, 138.90, 134.94, 134.43, 132.20, 131.36, 129.62, 129.19, 128.91, 128.61, 128.21, 127.77, 127.72, 126.96, 126.92, 59.39, 51.97, 45.51, 43.27, 35.51, 35.27.

4-(4-(Azetidin-3-yl)phenyl)-7-(4-(trifluoromethyl)phenyl)-2-naphthoic Acid (5).

Procedure A.: LiOH (7.4 mg, 0.3 mmol) was added to a solution of **23** (6.25 mg, 0.013 mmol) in THF-H₂O MeOH (3:1:1, 1 mL). The resulting mixture was sonicated for 30 s and stirred at rt for 3 h. The reaction was quenched and neutralized by 1 M HCl. Volatiles were evaporated, and the residue was purified by RP-HPLC (C18, A: ACN, B: 10 mM TEAA, 45% → 60% A in 40 min, flow rate = 5 mL/min, t_R = 17.2 min) to give **5** as a white powder (2.73 mg, 47%): ¹H NMR (400 MHz, CD₃OD) δ 8.76 (s, 1H), 8.44 (d, J = 2.0 Hz, 1H), 8.04–7.96 (m, 4H), 7.93 (dd, J = 8.8, 1.9 Hz, 1H), 7.81 (d, J = 8.1 Hz, 2H), 7.60 (s, 4H), 4.53–4.31 (m, 5H). HRMS m/z [M + H]⁺ for C₂₇H₂₁NO₂F₃ calculated 448.1524, found 448.1520.

4-(4-(2-Azaspiro[3.3]heptan-6-yl)phenyl)-7-(4-(trifluoromethyl)phenyl)-2-naphthoic Acid (6).

Procedure B.: Pd/C (10%, 3 mg) was added to a solution of **7** (0.0016 mmol) in DMF (0.3 mL). The resulting mixture was bubbled with H₂ at rt for 5 h. The Pd/C was filtered. Volatiles were evaporated, and the residue was purified by RP-HPLC (C18, A: ACN, B: 10 mM TEAA, 45% → 60% A in 40 min, flow rate = 5 mL/min, t_R = 20 min) to give **6** as a white powder (0.4 mg, 51%): ¹H NMR (400 MHz, CD₃OD) δ 8.74 (s, 1H), 8.43 (d, J = 2.0 Hz, 1H), 8.01 (dd, J = 8.7, 3.6 Hz, 3H), 7.96–7.89 (m, 2H), 7.81 (d, J = 8.1 Hz, 2H), 7.48 (d, J = 8.0 Hz, 2H), 7.42 (d, J = 8.0 Hz, 2H), 4.30 (s, 2H), 4.07 (s, 2H), 3.62–3.60 (m, 1H), 2.83–2.75 (m, 2H), 2.51 (td, J = 9.7, 2.9 Hz, 2H). HRMS m/z [M + H]⁺ for C₃₀H₂₅NO₂F₃ calculated 488.1837, found 488.1833.

4-(4-(2-Azaspiro[3.3]hept-5-en-6-yl)phenyl)-7-(4-(trifluoromethyl)phenyl)-2-naphthoic Acid (7), 4-(4-(6-Hydroxy-2-azaspiro[3.3]heptan-6-yl)phenyl)-7-(4-(trifluoromethyl)phenyl)-2-naphthoic Acid (8), and 4-(4-(6-Methoxy-2-azaspiro[3.3]heptan-6-yl)phenyl)-7-(4-(trifluoromethyl)phenyl)-2-naphthoic Acid, and 4-(4-(6-(Methoxy-d₃)-2-azaspiro[3.3]heptan-6-yl)phenyl)-7-(4-(trifluoromethyl)phenyl)-2-naphthoic Acid (6:4, 9).—A TFA solution in THF (67%, 4.5 mL) was added to **27** (entire residue from hydrolysis of **26**, 0.057 mmol). The resulting mixture was stirred at rt for 1 h. The stir bar was washed with MeOH. Volatiles were evaporated, and the residue was dissolved in CD₃OD for crude NMR. CD₃OD was removed and the residue was purified by RP-HPLC (C18, A: ACN, B: 10 mM TEAA, 45% → 60% A in 40 min, flow rate = 5 mL/min) to give **7** (1.8 mg, 7%, t_R = 42.4 min), **8** (2.54 mg, 9%, t_R = 33.0 min), and **9** (10.5 mg, 36%, t_R = 40.6 min). **7** has: ¹H NMR (400 MHz, CD₃OD) δ 8.76 (s, 1H), 8.43 (d, J = 1.9 Hz, 1H), 8.04–7.97

(m, 4H), 7.97–7.91 (m, 1H), 7.81 (d, J = 8.1 Hz, 2H), 7.62 (d, J = 7.9 Hz, 2H), 7.56 (d, J = 8.0 Hz, 2H), 6.55 (s, 1H), 4.42–4.31 (m, 4H), 3.20 (s, 2H). HRMS m/z [M + H]⁺ for C₃₀H₂₃NO₂F₃ calculated 486.1681, found 486.1682. **8** has: ¹H NMR (400 MHz, CD₃OD) δ 8.72 (s, 1H), 8.41 (d, J = 1.9 Hz, 1H), 7.99 (d, J = 8.7 Hz, 4H), 7.90 (dd, J = 8.9, 1.9 Hz, 1H), 7.80 (d, J = 8.1 Hz, 2H), 7.62 (d, J = 8.0 Hz, 2H), 7.54 (d, J = 7.9 Hz, 2H), 4.30 (s, 2H), 4.09 (s, 2H), 2.94 (d, J = 13.0 Hz, 2H), 2.66 (d, J = 12.5 Hz, 2H). HRMS m/z [M + H]⁺ for C₃₀H₂₅NO₃F₃ calculated 504.1787, found 504.1796. **9** has: ¹H NMR (600 MHz, CD₃OD) δ 8.77–8.74 (m, 1H), 8.44 (d, J = 1.9 Hz, 1H), 8.05–8.00 (m, 4H), 7.94 (dd, J = 8.8, 2.0 Hz, 1H), 7.83 (d, J = 8.2 Hz, 2H), 7.63–7.55 (m, 4H), 4.27 (s, 2H), 4.08 (s, 2H), 3.07 (s, 2H), 2.91–2.84 (m, 2H), 2.80–2.74 (m, 2H). HRMS m/z [M + H]⁺ for C₃₁H₂₇NO₃F₃ calculated 518.1943, found 518.1939; for C₃₁H₂₄D₃NO₃F₃ calculated 521.2117, found 521.2126.

rac-4-(4-((3aR,6aR)-5-Hydroxyoctahydrocyclopenta[c]pyrrol-5-yl)phenyl)-7-(4-(trifluoromethyl)phenyl)-2-naphthoic Acid (11).—Pd/C (10%, 53 mg) was added

to a solution of **31** (10.7 mg, 0.0177 mmol) in DMF (5 mL). The resulting mixture was bubbled with H₂ at rt for 5 h. The Pd/C was filtered. The filtrate was purified by RP-HPLC (C18, A: ACN, B: 10 mM TEAA, 30% → 50% A in 40 min, flow rate = 5 mL/min, t_R = 35 min) to give **11** as a white powder (3.18 mg, 35% overall yield from **30**): ¹H NMR (400 MHz, CD₃OD) δ 8.75 (s, 1H), 8.43 (d, J = 2.0 Hz, 1H), 8.05–7.96 (m, 4H), 7.93 (dd, J = 9.0, 2.0 Hz, 1H), 7.81 (d, J = 8.1 Hz, 2H), 7.69 (d, J = 8.2 Hz, 2H), 7.54 (d, J = 8.0 Hz, 2H), 3.56–3.46 (m, 2H), 2.98 (t, J = 11.2 Hz, 2H), 2.76–2.65 (m, 1H), 2.60–2.45 (m, 2H), 2.22 (dd, J = 12.6, 5.4 Hz, 1H), 2.06–1.95 (m, 2H). ¹³C NMR (126 MHz, MeOD) δ 149.68, 145.31, 141.54, 139.73, 138.88, 134.98, 134.44, 132.11, 130.90, 129.18, 128.92, 128.54, 127.80, 126.93, 125.82, 116.40, 90.29, 52.72, 50.48, 47.94, 47.45, 45.07, 44.61, 40.43. HRMS m/z [M + H]⁺ for C₃₁H₂₇NO₃F₃ calculated 518.1943, found 518.1944.

rac-4-(4-((3aR,6aR)-1,2,3,3a,4,6a-Hexahydrocyclopenta[c]-pyrrol-5-yl)phenyl)-7-(4-(trifluoromethyl)phenyl)-2-naphthoic Acid (12).—A

solution of **11** (0.012 mmol, crude reaction residue without HPLC purification) in TFA (2 mL) was refluxed in a 90 °C oil bath for 2 h. Volatiles were evaporated, and the residue was purified by RPHPLC (C18, A: ACN, B: 10 mM TEAA, 45% → 60% A in 40 min, flow rate = 5 mL/min, t_R = 21 min) to give **12** as a white powder (1.9 mg, 33% overall yield from **31**): ¹H NMR (400 MHz, CD₃OD) δ 8.75 (s, 1H), 8.43 (d, J = 2.0 Hz, 1H), 8.07–7.96 (m, 4H), 7.94 (dd, J = 8.9, 2.0 Hz, 1H), 7.81 (d, J = 8.1 Hz, 2H), 7.68 (d, J = 8.1 Hz, 2H), 7.53 (d, J = 8.0 Hz, 2H), 6.61 (s, 1H), 3.62 (d, J = 3.3 Hz, 1H), 3.53 (dd, J = 10.2, 6.5 Hz, 1H), 3.26–3.15 (m, 1H), 3.04 (d, J = 7.0 Hz, 2H), 2.99 (dd, J = 14.4, 6.0 Hz, 1H), 2.68–2.55 (m, 1H), 2.40 (dq, J = 11.9, 5.9 Hz, 1H). HRMS m/z [M + H]⁺ for C₃₁H₂₅NO₂F₃ calculated 500.1837, found 500.1834.

rac-4-(4-((3aR,6aR)-Octahydrocyclopenta[c]pyrrol-5-yl)phenyl)-7-(4-(trifluoromethyl)phenyl)-2-naphthoic Acid (13).—Treatment of **12**

(0.021 mmol, crude reaction residue without HPLC purification) by using Procedure B gave **13** (0.57 mg, 5% overall yield from **31**) as a white powder: ¹H NMR (400 MHz, CD₃OD) δ 8.74 (s, 1H), 8.42 (d, J = 1.9 Hz, 1H), 8.06–7.95 (m, 4H), 7.93 (d, J = 8.4 Hz, 1H), 7.81 (d, J = 8.0 Hz, 2H), 7.49 (s, 4H), 4.01 (d, J = 9.2 Hz, 1H), 3.48 (p, J = 6.4 Hz, 2H), 3.03–2.86

(m, 2H), 2.59 (dd, $J = 12.8, 6.4$ Hz, 1H), 2.47–2.29 (m, 2H), 2.17–1.98 (m, 2H), 1.64 (q, $J = 11.0$ Hz, 1H). HRMS m/z $[M + H]^+$ for $C_{31}H_{27}NO_2F_3$ calculated 502.1994, found 502.1986.

4-(4-((1R,5S,6r)-3-Azabicyclo[3.1.1]heptan-6-yl)phenyl)-7-(4-(trifluoromethyl)phenyl)-2-naphthoic Acid (14).—

Concentrated sulfuric acid (95–98%, 0.9 mL) was added to a mixture of **15** (9 mg, 0.015 mmol) and $NaBH_4$ (5.7 mg, 0.15 mmol) in THF (0.1 mL) under argon (caution, running the reaction under argon is required to avoid fire/explosion). The resulting solution was stirred at rt for 30 min. The mixture was basified with cold 6 N NaOH aqueous solution and extracted with ethyl acetate three times. The organic layer was dried over anhydrous Na_2SO_4 . Volatiles were evaporated, and the residue was purified by RP-HPLC (C18, A: ACN, B: 10 mM TEAA, 35% → 55% A in 40 min, flow rate = 5 mL/min, $t_R = 38.8$ min) to give **14** as a white powder (0.8 mg, 11%): 1H NMR (400 MHz, CD_3OD) δ 8.76 (s, 1H), 8.44 (d, $J = 2.0$ Hz, 1H), 8.07–7.96 (m, 4H), 7.96–7.90 (m, 1H), 7.81 (d, $J = 8.1$ Hz, 2H), 7.56 (d, $J = 7.8$ Hz, 2H), 7.38 (d, $J = 7.7$ Hz, 2H), 4.09 (q, $J = 9.6$ Hz, 1H), 3.62 (t, $J = 7.2$ Hz, 1H), 3.42–3.33 (m, 3H), 3.23 (dd, $J = 16.7, 7.1$ Hz, 2H), 2.74 (q, $J = 9.1$ Hz, 1H), 2.33 (q, $J = 10.5$ Hz, 1H). HRMS m/z $[M + H]^+$ for $C_{30}H_{24}F_3NO_2$ calculated 488.1837, found 488.1829.

4-(4-((1R,5S,6r)-6-Hydroxy-3-azabicyclo[3.1.1]heptan-6-yl)-phenyl)-7-(4-(trifluoromethyl)phenyl)-2-naphthoic Acid (15).

Procedure C.: A TFA solution in THF (67%, 2 mL) was added to **35** (0.022 mmol, reaction residue). The resulting mixture was stirred at rt for 1 h. Volatiles were evaporated, and the residue was purified by RPHPLC (C18, A: ACN, B: 10 mM TEAA, 35% → 55% A in 40 min, flow rate = 5 mL/min, $t_R = 27.7$ min) to give **15** (4.6 mg, 42%) as a white solid: 1H NMR (400 MHz, DMSO) δ 8.76 (s, 1H), 8.65 (d, $J = 2.0$ Hz, 1H), 8.06 (t, $J = 8.2$ Hz, 3H), 7.98 (d, $J = 8.9$ Hz, 1H), 7.92–7.85 (m, 3H), 7.73 (d, $J = 7.9$ Hz, 2H), 7.59 (d, $J = 7.8$ Hz, 2H), 3.69 (d, $J = 11.7$ Hz, 2H), 3.47 (d, $J = 11.9$ Hz, 2H), 2.89 (d, $J = 4.5$ Hz, 2H), 1.71 (s, 2H). ^{13}C NMR (126 MHz, MeOD) δ 168.27, 143.84, 142.24, 139.99, 139.55, 137.54, 133.56, 132.98, 130.93, 129.88, 128.21, 127.82, 127.52, 127.27, 126.39, 126.32, 125.56, 125.53, 73.18, 44.35, 39.91, 20.75. HRMS m/z $[M + H]^+$ for $C_{30}H_{25}NO_3F_3$ calculated 504.1787, found 504.1793.

4-(4-(Azepan-4-yl)phenyl)-7-(4-(trifluoromethyl)phenyl)-2-naphthoic Acid (16).

—Treatment of **17** (0.038 mmol, crude reaction residue without HPLC purification) by using Procedure B gave **16** (4 mg, 22% overall yield from **38**) as a white powder: 1H NMR (400 MHz, CD_3OD) δ 8.77–8.72 (m, 1H), 8.42 (d, $J = 1.9$ Hz, 1H), 8.05–7.95 (m, 4H), 7.92 (dd, $J = 8.9, 1.9$ Hz, 1H), 7.81 (d, $J = 8.1$ Hz, 2H), 7.48 (q, $J = 8.1$ Hz, 4H), 3.54–3.35 (m, 4H), 3.02 (t, $J = 10.9$ Hz, 1H), 2.22 (d, $J = 15.9$ Hz, 4H), 2.09–1.86 (m, 2H). HRMS m/z $[M + H]^+$ for $C_{30}H_{27}NO_2F_3$ calculated 490.1994, found 490.1992.

Mixture of 4-(4-(2,3,6,7-Tetrahydro-1H-azepin-4-yl)phenyl)-7-(4-(trifluoromethyl)phenyl)-2-naphthoic Acid and 4-(4-(2,5,6,7-Tetrahydro-1H-azepin-4-yl)phenyl)-7-(4-(trifluoromethyl)phenyl)-2-naphthoic Acid (17).—

Treatment of **39** (all residue from hydrolysis of **38**, 0.057 mmol) by using Procedure C gave **17** (5.08 mg, 18%) as a mixture of two constitutional isomers (1:1): 1H NMR (400

MHz, CD₃OD) δ 8.76 (d, J = 2.8 Hz, 1H), 8.43 (d, J = 2.4 Hz, 1H), 8.05–7.97 (m, 4H), 7.972–7.90 (m, 1H), 7.81 (d, J = 8.1 Hz, 2H), 7.66–7.49 (m, 4H), 6.35 (t, J = 6.2 Hz, 0.5H), 6.21 (t, J = 6.5 Hz, 0.5H), 3.99 (d, J = 6.5 Hz, 1H), 3.59–3.49 (m, 1H), 3.48–3.41 (m, 1H), 3.39–3.32 (m, 1H), 3.14–3.05 (m, 1H), 3.06–2.99 (m, 1H), 2.74 (d, J = 5.5 Hz, 1H), 2.14 (d, J = 5.7 Hz, 1H). HRMS m/z [M + H]⁺ for C₃₀H₂₅NO₂F₃ calculated 488.1837, found 488.1835.

4-(4-(Azocan-5-yl)phenyl)-7-(4-(trifluoromethyl)phenyl)-2-naphthoic Acid (18).

—Treatment of **47** (6 mg, 0.0112 mmol) by using Procedure A gave **18** (3 mg, overall yield 54% from **45**): ¹H NMR (400 MHz, MeOD) δ 8.73 (s, 1H), 8.41 (d, J = 1.9 Hz, 1H), 8.06–7.95 (m, 4H), 7.92 (dd, J = 8.9, 2.0 Hz, 1H), 7.80 (d, J = 8.2 Hz, 2H), 7.47 (d, J = 8.2 Hz, 2H), 7.43 (d, J = 8.2 Hz, 2H), 3.46–3.37 (m, 2H), 3.36–3.32 (m, 2H), 3.06–2.95 (m, 1H), 2.27–2.09 (m, 4H), 2.07–1.96 (m, 4H). ¹³C NMR (126 MHz, MeOD) δ 168.58, 148.12, 143.92, 140.30, 137.68, 137.43, 133.56, 133.08, 130.61, 129.85, 127.74, 127.51, 127.10, 126.63, 126.46, 126.35, 125.54, 114.99, 46.54, 45.17, 32.49, 23.09. HRMS m/z [M + H]⁺ for C₃₁H₂₉NO₂F₃ calculated 504.2150, found 504.2141.

4-(4-(1,2,3,4,7,8-Hexahydroazocin-5-yl)phenyl)-7-(4-(trifluoromethyl)phenyl)-2-naphthoic Acid (19) and 4-(4-(5-Hydroxyazocan-5-yl)phenyl)-7-(4-(trifluoromethyl)phenyl)-2-naphthoic Acid (20).

—Treatment of **43** (all residue from hydrolysis of **42**, 0.049 mmol) by using Procedure C gave **19** (4.52 mg, 18%) in addition to **20** (4.67 mg, 18%). **19** has: ¹H NMR (400 MHz, CD₃OD) δ 8.72 (s, 1H), 8.40 (d, J = 2.0 Hz, 1H), 8.03–7.95 (m, 5H), 7.90 (dd, J = 9.0, 2.0 Hz, 1H), 7.78 (d, J = 8.1 Hz, 3H), 7.66 (d, J = 8.0 Hz, 3H), 7.51 (d, J = 8.0 Hz, 2H), 6.28 (t, J = 8.3 Hz, 1H), 3.35–3.28 (m, 2H), 3.25–3.21 (m, 2H), 2.90 (t, J = 6.3 Hz, 2H), 2.72 (dd, J = 12.0, 7.5 Hz, 2H), 2.08 (s, 2H). HRMS m/z [M + H]⁺ for C₃₁H₂₆NO₂F₃ calculated 502.1994, found 502.2001. **20** has: ¹H NMR (400 MHz, CD₃OD) δ 8.75 (s, 1H), 8.42 (d, J = 1.9 Hz, 1H), 8.00–7.94 (m, 4H), 7.91 (dd, J = 8.9, 1.9 Hz, 1H), 7.78 (d, J = 8.1 Hz, 2H), 7.70 (d, J = 8.4 Hz, 2H), 7.65 (d, J = 8.5 Hz, 2H), 3.85 (dt, J = 13.3, 7.0 Hz, 2H), 3.41 (dt, J = 12.5, 6.7 Hz, 2H), 2.70 (dt, J = 13.5, 6.8 Hz, 2H), 2.47 (dt, J = 13.5, 6.7 Hz, 2H), 2.35 (dp, J = 13.7, 6.8 Hz, 2H), 2.24 (dq, J = 13.5, 6.8 Hz, 2H). HRMS m/z [M – OH]⁺ for C₃₁H₂₇NO₂F₃ calculated 502.1994, found 502.1993.

Ethyl 4-(4-(Azetidin-3-yl)phenyl)-7-(4-(trifluoromethyl)phenyl)-2-naphthoate (23).

Procedure D.: To a vacuum-dried mixture of **21** (5.8 mg, 0.023 mmol), **22**⁴¹ (11 mg, 0.023 mmol), Pd(PPh₃)₄ (2.7 mg, 0.0023 mmol), and Na₂CO₃ (6 mg, 0.057 mmol) was added sonicated 1,2-dimethoxyethane-water (4:1, 1 mL). The reaction mixture was degassed with argon for 10 min and then stirred at 80 °C overnight. Volatiles were evaporated, and the residue was column-chromatographed (CH₂Cl₂/MeOH/TEA, 100:0:1 → 90:10:1) to give **23** (6.25 mg, 57%): ¹H NMR (400 MHz, CDCl₃) δ 8.68 (s, 1H), 8.22 (d, J = 1.9 Hz, 1H), 8.01 (d, J = 1.7 Hz, 1H), 7.97 (d, J = 8.8 Hz, 1H), 7.86–7.77 (m, 3H), 7.75 (d, J = 8.3 Hz, 2H), 7.61 (d, J = 7.9 Hz, 2H), 7.55 (d, J = 8.0 Hz, 2H), 4.57–4.41 (m, 5H), 3.15 (q, J = 7.3 Hz, 2H), 1.44 (td, J = 7.2, 4.1 Hz, 3H). HRMS m/z [M + H]⁺ for C₃₂H₂₉NO₂F₃ calculated

516.2150, found 516.2145. HRMS m/z $[M + H]^+$ for $C_{29}H_{25}NO_2F_3$ calculated 476.1837, found 476.1837.

tert-Butyl 6-(4-Bromophenyl)-6-hydroxy-2-azaspiro[3.3]heptane-2-carboxylate (25).

Procedure E.: A mixture of 1,4-dibromobenzene (2.9 g, 12.5 mmol) and magnesium turnings (60.8 mg, 2.5 mmol) in THF (5 mL) was sonicated for 2 h. The solution was cooled to 0 °C. Into the Grignard reagent was added the solution of **24** (105.6 mg, 0.5 mmol) in THF (10 mL). The resulting mixture was stirred at 0 °C to rt overnight. The residue was partitioned between ethyl acetate and aqueous $NaHCO_3$. The organic layer was dried over anhydrous Na_2SO_4 . Volatiles were evaporated, and the residue was column-chromatographed (hexane/ethyl acetate = 80:20 → 40:60) to give **25** (72.3 mg; 39%): 1H NMR (400 MHz, $CDCl_3$) δ 7.50–7.44 (m, 2H), 7.29–7.24 (m, 2H), 4.05 (s, 2H), 3.78 (s, 2H), 2.72–2.66 (m, 2H), 2.52 (d, $J = 12.7$ Hz, 2H), 1.41 (s, 9H). HRMS m/z $[M - t\text{-butyl} + 2H]^+$ for $C_{13}H_{15}N^{79}BrO_3$ calculated 312.0235, found 312.0234.

tert-Butyl 6-(4-(3-(Ethoxycarbonyl)-6-(4-(trifluoromethyl)-phenyl)naphthalen-1-yl)phenyl)-6-hydroxy-2-azaspiro[3.3]heptane-2-carboxylate (26).—Treatment of

25 (25.6 mg, 0.07 mmol) by using Procedure D gave **26** (36.12 mg, 82%): 1H NMR (400 MHz, $CDCl_3$) δ 8.68 (s, 1H), 8.22 (d, $J = 1.8$ Hz, 1H), 8.06–7.96 (m, 2H), 7.81 (d, $J = 8.1$ Hz, 2H), 7.76 (td, $J = 6.8, 3.3$ Hz, 3H), 7.57 (d, $J = 8.0$ Hz, 2H), 7.52 (d, $J = 8.1$ Hz, 2H), 4.46 (q, $J = 7.1$ Hz, 2H), 4.13 (s, 2H), 3.90 (s, 2H), 2.87 (d, $J = 12.8$ Hz, 2H), 2.64 (d, $J = 12.6$ Hz, 2H), 1.44 (d, $J = 9.7$ Hz, 12H). HRMS m/z $[M + Na]^+$ for $C_{37}H_{36}NO_5F_3Na$ calculated 654.2443, found 654.2446.

4-(4-(2-(tert-Butoxycarbonyl)-6-hydroxy-2-azaspiro[3.3]heptan-6-yl)phenyl)-7-(4-(trifluoromethyl)phenyl)-2-naphthoic Acid (27)—Treatment of **26** (36 mg, 0.057 mmol) by using

Procedure A (without HPLC purification) gave **27** of sufficient purity to be used in next step: 1H NMR (400 MHz, CD_3OD) δ 8.50 (s, 1H), 8.21 (s, 1H), 7.91–7.80 (m, 4H), 7.67 (dd, $J = 14.7, 9.8$ Hz, 3H), 7.52–7.45 (m, 2H), 7.37 (t, $J = 5.3$ Hz, 2H), 3.98 (s, 2H), 3.76 (s, 2H), 2.73 (d, $J = 12.1$ Hz, 2H), 2.52–2.45 (m, 2H), 1.32 (d, $J = 3.8$ Hz, 9H). HRMS m/z $[M + Na]^+$ for $C_{35}H_{32}NO_5F_3Na$ calculated 626.2130, found 626.2136.

rac-(3aR, 6aR)-2-Benzyl-5-(4-bromophenyl)-octahydrocyclopenta[c]pyrrol-5-ol (29).—Treatment of **28** (125.9 mg, 0.5 mmol) by using Procedure E (column

chromatography; DCM/ MeOH, 100:0 → 95:5) gave **29** (101.18 mg, 54%): 1H NMR (400 MHz, $CDCl_3$) δ 7.48–7.40 (m, 2H), 7.40–7.20 (m, 7H), 3.94–3.78 (m, 2H), 2.88 (dq, $J = 9.6, 4.5$ Hz, 2H), 2.80 (s, 1H), 2.50 (tdt, $J = 16.7, 11.3, 8.9$ Hz, 3H), 2.29 (dd, $J = 12.7, 7.1$ Hz, 1H), 2.18 (dtd, $J = 16.1, 11.4, 5.6$ Hz, 1H), 1.97 (dd, $J = 12.6, 4.7$ Hz, 1H), 1.76–1.61 (m, 2H). HRMS m/z $[M + H]^+$ for $C_{20}H_{23}NO^{79}Br$ calculated 372.0963, found 372.0966.

rac-Ethyl 4-(4-((3aR,6aR)-2-benzyl-5-hydroxyoctahydrocyclopenta[c]pyrrol-5-yl)phenyl)-7-(4-(trifluoromethyl)phenyl)-2-naphthoate (30).—Treatment of **29**

(26.1 mg, 0.07 mmol) by using Procedure D gave **30** (33.7 mg, 76%): 1HNMR

(400 MHz, CDCl₃) δ 8.65 (s, 1H), 8.20 (d, J = 1.9 Hz, 1H), 8.04–7.95 (m, 2H), 7.79 (d, J = 8.2 Hz, 2H), 7.76–7.68 (m, 3H), 7.60 (d, J = 8.1 Hz, 2H), 7.54 (d, J = 7.4 Hz, 2H), 7.48 (d, J = 8.0 Hz, 2H), 7.36 (dt, J = 13.7, 7.2 Hz, 3H), 4.44 (q, J = 7.1 Hz, 2H), 4.14 (s, 2H), 3.32–3.17 (m, 2H), 2.99–2.76 (m, 3H), 2.57–2.42 (m, 2H), 2.20 (dd, J = 12.6, 5.2 Hz, 1H), 1.94 (dt, J = 17.9, 12.1 Hz, 2H), 1.44 (t, J = 7.1 Hz, 3H). HRMS m/z [M + H]⁺ for C₄₀H₃₇NO₃F₃ calculated 636.2726, found 636.2724.

rac-4-(4-((3aR,6aR)-2-Benzyl-5-hydroxyoctahydrocyclopenta[c]-pyrrol-5-yl)phenyl)-7-(4-(trifluoromethyl)phenyl)-2-naphthoic Acid (31).—Treatment

of **30** (33.7 mg, 0.053 mmol) by using Procedure A

(without HPLC purification) gave **31** of sufficient purity to be used

in next step: ¹H NMR (400 MHz, CD₃OD) δ 8.59 (s, 1H), 8.30 (s, 1H), 8.00 (s, 1H), 7.92 (dd, J = 8.5, 5.3 Hz, 3H), 7.74 (d, J = 7.5 Hz, 3H), 7.65 (dd, J = 15.8, 6.5 Hz, 4H), 7.51–7.39 (m, 5H), 4.62–4.50 (m, 2H), 3.54 (d, J = 12.9 Hz, 2H), 3.22 (q, J = 13.9 Hz, 2H), 2.94–2.66 (m, 2H), 2.47 (dd, J = 13.2, 7.1 Hz, 1H), 2.18 (dd, J = 12.8, 5.0 Hz, 1H), 1.97 (q, J = 11.3 Hz, 2H). HRMS m/z [M + H]⁺ for C₃₈H₃₃NO₃F₃ calculated 608.2413, found 608.2408.

tert-Butyl (1R,5S,6r)-6-(4-Bromophenyl)-6-hydroxy-3-

azabicyclo[3.1.1]heptane-3-carboxylate (33).—Treatment of **32** (105.65 mg, 0.5

mmol) by using Procedure E gave **33** (99.36 mg, 54%): ¹H NMR (400 MHz, CDCl₃) δ 7.50 (dd, J = 8.7, 2.3 Hz, 2H), 7.39 (d, J = 8.5 Hz, 2H), 3.82–3.66 (m, 4H), 2.82–2.76 (m, 1H), 2.71–2.63 (m, 1H), 1.55 (dt, J = 11.4, 6.2 Hz, 1H), 1.45 (d, J = 2.5 Hz, 9H), 1.33 (d, J = 10.1 Hz, 1H). HRMS m/z [M - *t*-butyl + 2H]⁺ for C₁₃H₁₅N⁷⁹BrO₃ calculated 312.0235, found 312.0234.

tert-Butyl

(1R,5S,6r)-6-(4-(3-(Ethoxycarbonyl)-6-(4-(trifluoromethyl)phenyl)naphthalen-1-yl)phenyl)-6-hydroxy-3-azabicyclo[3.1.1]heptane-3-carboxylate (34).—Treatment

of **33** (25.8 mg, 0.07 mmol) by using Procedure D gave **34** (41 mg, 93%): ¹H NMR (400 MHz, CDCl₃) δ 8.69 (d, J = 1.6 Hz, 1H), 8.23 (d, J = 1.9 Hz, 1H), 8.07–8.01 (m, 2H), 7.81 (d, J = 8.2 Hz, 2H), 7.79–7.73 (m, 3H), 7.71 (d, J = 8.0 Hz, 2H), 7.56 (d, J = 8.0 Hz, 2H), 4.45 (q, J = 7.1 Hz, 2H), 3.94–3.77 (m, 4H), 3.02–2.94 (m, 1H), 2.88 (d, J = 6.7 Hz, 1H), 1.74 (dt, J = 11.4, 6.1 Hz, 1H), 1.52 (s, 9H), 1.48–1.40 (m, 4H). HRMS m/z [M–Boc–O]⁺ for C₃₂H₂₇NO₂F₃ calculated 514.1994, found 514.2001.

4-(4-((1R,5S,6r)-3-(tert-Butoxycarbonyl)-6-hydroxy-3-azabicyclo[3.1.1]heptan-6-yl)phenyl)-7-(4-(trifluoromethyl)phenyl)-2-naphthoic Acid (35).—Treatment of **34** (41 mg, 0.065 mmol) by using

Procedure A (without HPLC purification) gave **35** of sufficient purity to be used in next step: ¹H NMR (400 MHz, CD₃OD) δ 8.58 (s, 1H), 8.31 (d, J = 1.9 Hz, 1H), 8.04 (d, J = 1.6 Hz, 1H), 7.97 (dd, J = 8.6, 3.2 Hz, 3H), 7.81–7.74 (m, 3H), 7.72 (d, J = 7.9 Hz, 2H), 7.53 (t, J = 6.6 Hz, 2H), 3.84–3.69 (m, 4H), 2.96–2.82 (m, 2H), 1.69 (dt, J = 11.1, 6.0 Hz, 1H), 1.36 (d, J = 9.7 Hz, 1H). MS m/z [M–Boc–O]⁺ for C₃₀H₂₃NO₂F₃ calculated 486.2, found 486.2.

tert-Butyl 4-(4-Bromophenyl)-4-hydroxyazepane-1-carboxylate (37).—Treatment of **36** (106.65 mg, 0.5 mmol) by using Procedure E gave **37** (135 mg, 73%): $^1\text{H NMR}$ (400 MHz, CDCl_3) δ 7.45 (d, $J = 8.0$ Hz, 2H), 7.32 (d, $J = 8.3$ Hz, 2H), 3.92–3.47 (m, 2H), 3.32 (d, $J = 11.3$ Hz, 2H), 2.27–1.67 (m, 7H), 1.47 (d, $J = 4.1$ Hz, 9H).

tert-Butyl 4-(4-(3-(Ethoxycarbonyl)-6-(4-(trifluoromethyl)-phenyl)naphthalen-1-yl)phenyl)-4-hydroxyazepane-1-carboxylate (38).—Treatment of **37** (38.9 mg, 0.105 mmol) by using Procedure D gave **38** (36.4 mg, 82%): $^1\text{H NMR}$ (400 MHz, CDCl_3) δ 8.67 (s, 1H), 8.22 (s, 1H), 8.03 (d, $J = 9.4$ Hz, 2H), 7.81 (d, $J = 8.1$ Hz, 2H), 7.74 (d, $J = 8.0$ Hz, 3H), 7.62 (d, $J = 8.1$ Hz, 2H), 7.55–7.45 (m, 2H), 4.46 (q, $J = 7.1$ Hz, 2H), 3.93–3.53 (m, 2H), 3.45–3.34 (m, 2H), 2.35–2.05 (m, 3H), 1.99–1.68 (m, 4H), 1.51 (s, 9H), 1.45 (t, $J = 7.2$ Hz, 3H). HRMS m/z $[\text{M} + \text{Na}]^+$ for $\text{C}_{37}\text{H}_{38}\text{NO}_5\text{F}_3\text{Na}$ calculated 656.2600, found 656.2589.

4-(4-(1-(tert-Butoxycarbonyl)-4-hydroxyazepan-4-yl)phenyl)-7-(4-(trifluoromethyl)phenyl)-2-naphthoic Acid (39).—Treatment of **38** (36.4 mg, 0.057 mmol) by using Procedure A (without HPLC purification) gave **39** of sufficient purity to be used in next step: $^1\text{HNMR}$ (400 MHz, CD_3OD) δ 8.34 (s, 1H), 8.08 (s, 1H), 7.80 (s, 1H), 7.74 (d, $J = 8.1$ Hz, 3H), 7.55 (d, $J = 8.0$ Hz, 3H), 7.39 (d, $J = 8.1$ Hz, 2H), 7.25 (d, $J = 7.2$ Hz, 2H), 3.46 (s, 2H), 3.23–3.16 (m, 2H), 2.16–1.51 (m, 6H), 1.27 (s, 9H). MS m/z $[\text{M} - \text{Boc} - \text{O}]^+$ for $\text{C}_{30}\text{H}_{25}\text{NO}_2\text{F}_3$ calculated 488.1837, found 488.1840.

tert-Butyl 5-(4-Bromophenyl)-5-hydroxyazocane-1-carboxylate (41).—Treatment of **40** (113.65 mg, 0.5 mmol) by using Procedure E gave **41** (155 mg, 81%): $^1\text{H NMR}$ (400 MHz, CDCl_3) δ 7.44–7.39 (m, 2H), 7.37–7.32 (m, 2H), 3.46–3.24 (m, 4H), 2.06–1.77 (m, 6H), 1.58–1.45 (m, 2H), 1.44 (s, 9H). HRMS m/z $[\text{M} - t\text{-butyl} + \text{H} - \text{OH}^-]^+$ for $\text{C}_{14}\text{H}_{17}\text{N}^{79}\text{BrO}_2$ calculated 310.0443, found 310.0437.

tert-Butyl 5-(4-(3-(Ethoxycarbonyl)-6-(4-(trifluoromethyl)-phenyl)naphthalen-1-yl)phenyl)-5-hydroxyazocane-1-carboxylate (42).—Treatment of **41** (26.9 mg, 0.07 mmol) by using Procedure D gave **42** (35.5 mg, 78%): $^1\text{H NMR}$ (400 MHz, CDCl_3) δ 8.68 (s, 1H), 8.22 (d, $J = 1.9$ Hz, 1H), 8.072–8.00 (m, 2H), 7.81 (d, $J = 8.1$ Hz, 2H), 7.78–7.71 (m, 3H), 7.66 (d, $J = 8.1$ Hz, 2H), 7.54–7.47 (m, 2H), 4.46 (q, $J = 7.1$ Hz, 2H), 3.56–3.37 (m, 5H), 2.27–2.06 (m, 2H), 2.00 (d, $J = 14.6$ Hz, 4H), 1.71 (s, 2H), 1.50 (s, 9H), 1.45 (t, $J = 7.1$ Hz, 3H). MS m/z $[\text{M} - \text{Boc} - \text{O}]^+$ for $\text{C}_{33}\text{H}_{31}\text{NO}_2\text{F}_3$ calculated 530.2, found 530.2.

4-(4-(1-(tert-Butoxycarbonyl)-5-hydroxyazocan-5-yl)phenyl)-7-(4-(trifluoromethyl)phenyl)-2-naphthoic Acid (43).—Treatment of **42** (32 mg, 0.049 mmol) by using Procedure A (without HPLC purification) gave **43** of sufficient purity to be used in next step: $^1\text{HNMR}$ (400 MHz, CD_3OD) δ 8.57 (s, 1H), 8.32–8.28 (m, 1H), 8.05–8.01 (m, 1H), 7.96 (d, $J = 8.3$ Hz, 3H), 7.82–7.73 (m, 3H), 7.67 (d, $J = 7.9$ Hz, 2H), 7.46 (d, $J = 7.9$ Hz, 2H), 3.56 (q, $J = 11.3$ Hz, 2H), 3.45–3.28 (m, 2H), 2.27–1.87 (m, 6H), 1.67–1.53 (m, 2H), 1.49 (s, 9H). MS m/z $[\text{M} - \text{Boc} - \text{O}]^+$ for $\text{C}_{31}\text{H}_{27}\text{NO}_2\text{F}_3$ calculated 502.1994, found 502.1990.

tert-Butyl 5-(4-Bromophenyl)-3,4,7,8-tetrahydroazocine-1(2H)-carboxylate (44).—Triphosgene (34.7 mg, 0.117 mmol) was added into a solution of **41** (30 mg, 0.078 mmol)

and DMAP (28.6 mg, 0.234 mmol) in DMF (2 mL). The resulting solution was stirred at rt for 2 h. Volatiles were evaporated, and the residue was column-chromatographed (hexane/ethyl acetate = 70:30 → 60:40) to give **44** (28 mg, quantitative): $^1\text{H NMR}$ (400 MHz, CDCl_3) δ 7.41 (d, J = 8.1 Hz, 2H), 7.29–7.22 (m, 2H), 6.13–6.02 (m, 1H), 3.50–3.35 (m, 2H), 3.21 (dt, J = 12.2, 6.0 Hz, 2H), 2.54 (hept, J = 6.1 Hz, 2H), 2.35 (dq, J = 13.6, 6.4 Hz, 2H), 1.99–1.72 (m, 2H), 1.44 (s, 9H). HRMS m/z $[\text{M}-\text{Boc}+2\text{H}]^+$ for $\text{C}_{13}\text{H}_{17}\text{N}^{79}\text{Br}$ calculated 266.0544, found 266.0543.

tert-Butyl 5-(4-(3-(Ethoxycarbonyl)-6-(4-(trifluoromethyl)-phenyl)naphthalen-1-yl)phenyl)-3,4,7,8-tetrahydroazocine-1(2H)-carboxylate (45).—Treatment of **44** (8.9 mg, 0.024 mmol) by using Procedure D gave **45** (15 mg, quantitative): $^1\text{H NMR}$ (400 MHz, CDCl_3) δ 8.70–8.66 (m, 1H), 8.23 (d, J = 1.9 Hz, 1H), 8.06 (dd, J = 5.1, 3.2 Hz, 2H), 7.83 (d, J = 8.2 Hz, 2H), 7.80–7.73 (m, 3H), 7.58 (dd, J = 8.3, 2.2 Hz, 2H), 7.48 (d, J = 7.9 Hz, 2H), 6.25 (q, J = 8.2 Hz, 1H), 4.47 (q, J = 7.1 Hz, 2H), 3.56–3.42 (m, 2H), 3.30 (d, J = 13.7 Hz, 2H), 2.67 (dt, J = 9.7, 6.1 Hz, 2H), 2.50–2.37 (m, 2H), 2.07–1.89 (m, 2H), 1.49–1.42 (m, 12H). HRMS m/z $[\text{M}-\text{Boc}+2\text{H}]^+$ for $\text{C}_{33}\text{H}_{31}\text{NO}_2\text{F}_3$ calculated 530.2307, found 530.2303.

tert-Butyl 5-(4-(3-(Ethoxycarbonyl)-6-(4-(trifluoromethyl)-phenyl)naphthalen-1-yl)phenyl)azocane-1-carboxylate (46).—To a mixture of **45** (7 mg, 0.0112 mmol) and 10% Pd-C (21 mg) in MeOH/THF (2.1 mL, 1:2) was added triethylsilane (21 μL , 15.3 mg, 0.13 mmol). The resulting mixture was stirred at rt for 5 min. Another portion of triethylsilane (28 μL , 20.4 mg, 0.175 mmol) diluted in 1 mL of THF was added dropwise within 5 min. The mixture was stirred for 5 min. Pd-C was removed by filtration and volatiles were evaporated, and the residue was dried under high vacuum to give **46** (7 mg, quantitative), which was used for the next step without further purification. **46** has: $^1\text{H NMR}$ (400 MHz, CDCl_3) δ 8.67 (d, J = 1.6 Hz, 1H), 8.23 (d, J = 1.9 Hz, 1H), 8.10–8.02 (m, 2H), 7.83 (d, J = 8.1 Hz, 2H), 7.80–7.72 (m, 3H), 7.44 (d, J = 8.0 Hz, 2H), 7.30 (d, J = 7.9 Hz, 2H), 4.46 (q, J = 7.1 Hz, 2H), 3.74 (q, J = 7.6 Hz, 2H), 3.62 (d, J = 14.4 Hz, 1H), 3.30–3.17 (m, 2H), 2.95–2.79 (m, 1H), 2.02–1.80 (m, 6H), 1.53 (s, 9H), 1.45 (t, J = 7.1 Hz, 3H), 1.33–1.26 (m, 2H). HRMS m/z $[\text{M} + \text{H}]^+$ for $\text{C}_{38}\text{H}_{40}\text{NO}_4\text{F}_3\text{Na}$ calculated 654.2807, found 654.2811.

Ethyl 4-(4-(Azocan-5-yl)phenyl)-7-(4-(trifluoromethyl)phenyl)-2-naphthoate (47).—Treatment of **46** (all residue from reduction of **45**, 0.0112 mmol) by using Procedure C gave **47** (volatiles were removed and the residue was used for next step without purification; 6 mg, quantitative): $^1\text{H NMR}$ (400 MHz, CDCl_3) δ 8.67 (s, 1H), 8.22 (d, J = 2.0 Hz, 1H), 8.07–8.01 (m, 2H), 7.82 (d, J = 8.2 Hz, 2H), 7.80–7.73 (m, 3H), 7.47 (d, J = 7.3 Hz, 2H), 7.38 (d, J = 7.5 Hz, 2H), 4.46 (q, J = 7.1 Hz, 2H), 3.56–3.21 (m, 4H), 3.08–2.97 (m, 1H), 2.28–2.00 (m, 8H), 1.47–1.43 (m, 3H). MS m/z $[\text{M} + \text{H}]^+$ for $\text{C}_{33}\text{H}_{33}\text{NO}_2\text{F}_3$ calculated 532.2, found 532.2.

tert-Butyl (1R,5S,6r)-6-(4-(3-((2-(Dimethylamino)-2-oxoethoxy)-carbonyl)-6-(4-(trifluoromethyl)phenyl)naphthalen-1-yl)phenyl)-6-hydroxy-3-azabicyclo[3.1.1]heptane-3-carboxylate (48).—To a solution of **35**

(62 mg, 0.103 mmol) and Cs₂CO₃ (66.93 mg, 0.205 mmol) in DMF (5 mL) under an argon atmosphere was added 2-chloro-*N,N*-dimethylacetamide (19 μ L, 22.5 mg, 0.186 mmol). The reaction mixture was stirred at rt overnight. The reaction mixture was partitioned between ethyl acetate (5 mL) and water (5 mL), and the aqueous phase was extracted with ethyl acetate (2 \times 5 mL). The combined organic layers were dried over Na₂SO₄, filtered, and concentrated under pressure. The residue was purified by silica gel chromatography (hexane/ethyl acetate = 1:1 \rightarrow 0:10) to afford compound **48** (40 mg, 56%) as a white solid: ¹H NMR (400 MHz, CDCl₃) δ 8.79 (s, 1H), 8.23 (s, 1H), 8.11 (s, 1H), 8.04 (d, *J* = 8.8 Hz, 1H), 7.85–7.73 (m, 5H), 7.70 (d, *J* = 7.8 Hz, 2H), 7.56 (d, *J* = 7.8 Hz, 2H), 5.05 (s, 2H), 3.93–3.70 (m, 4H), 3.08 (s, 3H), 3.05–2.98 (m, 4H), 2.90–2.85 (m, 1H), 1.79–1.70 (m, 1H), 1.45–1.41 (m, 1H). HRMS *m/z* [M–Boc+H–OH]⁺ for C₃₄H₃₀N₂O₃F₃ calculated 571.2209, found 571.2205.

2-(Dimethylamino)-2-oxoethyl

4-(4-((1*R*,5*S*,6*r*)-6-hydroxy-3-azabicyclo[3.1.1]heptan-6-yl)phenyl)-7-(4-(trifluoromethyl)-phenyl)-2-naphthoate (**49**).—

A TFA solution in THF (67%, 4.5 mL) was added to **48** (40 mg, 0.058 mmol). The resulting mixture was stirred at rt for 1 h. Volatiles were evaporated, and the residue was purified by RP-HPLC (C18, A: ACN, B: 0.2% TFA, 50% \rightarrow 100% A in 40 min, flow rate = 5 mL/min, *t_R* = 21.6 min) to give **49** as a white powder (20 mg, 59%): ¹H NMR (400 MHz, DMSO) δ 8.83 (s, 1H), 8.72 (d, *J* = 1.9 Hz, 1H), 8.30 (s, 1H), 8.12–8.05 (m, 3H), 7.98 (d, *J* = 8.9 Hz, 1H), 7.94–7.86 (m, 3H), 7.74 (d, *J* = 7.9 Hz, 2H), 7.61 (d, *J* = 7.9 Hz, 2H), 6.15 (s, 1H), 5.11 (s, 2H), 3.70 (d, *J* = 11.7 Hz, 2H), 3.49 (d, *J* = 11.9 Hz, 2H), 3.00 (s, 3H), 2.90 (d, *J* = 6.0 Hz, 2H), 2.85 (s, 3H), 1.77–1.66 (m, 1H), 1.62 (d, *J* = 11.1 Hz, 1H). ¹³C NMR (126 MHz, MeOD) δ 169.06, 167.46, 145.15, 143.71, 141.52, 140.79, 139.09, 134.88, 134.56, 132.63, 131.28, 129.30, 128.93, 128.47, 127.80, 127.59, 126.98, 74.57, 63.09, 45.75, 41.31, 36.25, 35.88, 22.12. HRMS *m/z* [M + H]⁺ for C₃₄H₃₂N₂O₄F₃ calculated 589.2314, found 589.2321.

Ethyl (1*R*,5*S*,6*r*)-6-(4-(3-((2-(Dimethylamino)-2-oxoethoxy)-carbonyl)-6-(4-(trifluoromethyl)phenyl)naphthalen-1-yl)phenyl)-6-hydroxy-3-azabicyclo[3.1.1]heptane-3-carboxylate (**50**).—

To a solution of **49** (34 mg, 0.058 mmol) and *N,N*-diisopropylethylamine (40 μ L, 30 mg, 0.232 mmol) in DMF (5 mL) was added ethyl chloroformate (9 μ L, 10.4 mg, 0.1 mmol). The resulting mixture was stirred at rt overnight. The volatiles were removed, and the residue was column-chromatographed (hexane/EtOAc, 60:40 \rightarrow 0:100) to give **50** (23.8 mg, 62%) as a white solid: ¹H NMR (400 MHz, CDCl₃) δ 8.80 (s, 1H), 8.24 (s, 1H), 8.12 (s, 1H), 8.04 (d, *J* = 8.8 Hz, 1H), 7.85–7.74 (m, 5H), 7.71 (d, *J* = 7.8 Hz, 2H), 7.58 (d, *J* = 7.8 Hz, 2H), 5.05 (s, 2H), 4.22 (q, *J* = 7.2 Hz, 2H), 3.97–3.83 (m, 4H), 3.08 (s, 3H), 3.05–2.99 (m, 4H), 2.92 (s, 1H), 1.76 (t, *J* = 5.2 Hz, 1H), 1.46 (d, *J* = 10.5 Hz, 1H), 1.32 (t, *J* = 7.1 Hz, 3H). ¹³C NMR (126 MHz, MeOD) δ 167.64, 166.06, 157.23, 143.90, 143.73, 140.28, 138.79, 137.55, 133.43, 133.19, 131.11, 129.66, 127.82, 127.51, 127.01, 126.45, 126.39, 126.16, 125.55, 125.52, 73.37, 61.68, 61.06, 46.23, 45.89, 40.33, 40.21, 34.86, 34.48, 22.57, 13.74. HRMS *m/z* [M + Na]⁺ for C₃₇H₃₅F₃N₂O₆Na calculated 683.2345, found 683.2344.

4-(4-((1R,5S,6r)-3-(Ethoxycarbonyl)-6-hydroxy-3-azabicyclo-[3.1.1]heptan-6-yl)phenyl)-7-(4-(trifluoromethyl)phenyl)-2-naphthoic Acid (51).—To a solution of **15** (11 mg, 0.02 mmol) and TEA (8.4 μ L, 6.1 mg, 0.06 mmol) in DMF (0.5 mL) was added ethyl chloroformate (2.1 μ L, 2.39 mg, 0.022 mmol). The resulting mixture was stirred at rt overnight. Volatiles were evaporated, and the residue was purified by RP-HPLC (C18, A: ACN, B: 10 mM TEAA, 50% \rightarrow 100% A in 40 min, flow rate = 5 mL/min, t_R = 18.8 min) to give **51** as a white powder (2.00 mg, 17%): $^1\text{H NMR}$ (400 MHz, MeOD) δ 8.60 (s, 1H), 8.37 (d, J = 2.0 Hz, 1H), 8.07–7.96 (m, 4H), 7.84 (dd, J = 8.8, 1.9 Hz, 1H), 7.82–7.73 (m, 4H), 7.59 (d, J = 7.8 Hz, 2H), 4.18 (q, J = 7.1 Hz, 2H), 3.94–3.75 (m, 4H), 3.00–2.99 (m, 1H), 2.95–2.91 (m, 1H), 1.82–1.72 (m, 1H), 1.43 (d, J = 10.2 Hz, 1H), 1.32 (t, J = 7.1 Hz, 3H). HRMS m/z [M + H] $^+$ for C₃₃H₂₉F₃NO₅ calculated 576.1998, found 576.2004.

4-(4-(1-(Ethoxycarbonyl)piperidin-4-yl)phenyl)-7-(4-(trifluoromethyl)phenyl)-2-naphthoic Acid (61).—To a solution of **1** (570.6 mg, 1.2 mmol), TEA (501 μ L, 363.6 mg, 3.6 mmol), and LiOH (28.8 mg, 1.2 mmol) in DMF (30 mL) was added ethyl chloroformate (114.7 μ L, 130.2 mg, 1.2 mmol). The resulting mixture was stirred at rt overnight. Volatiles were evaporated, and the residue was purified by RP-HPLC (C18, A: ACN, B: 10 mM TEAA, 50% \rightarrow 70% A in 40 min, flow rate = 5 mL/min, t_R = 36 min) to give **61** as a white powder (414 mg, 63%): $^1\text{H NMR}$ (400 MHz, MeOD) δ 8.57 (s, 1H), 8.30 (d, J = 2.0 Hz, 1H), 7.98–7.89 (m, 4H), 7.80–7.70 (m, 3H), 7.40 (d, J = 7.9 Hz, 2H), 7.34 (d, J = 8.0 Hz, 2H), 4.26 (d, J = 13.1 Hz, 2H), 4.12 (q, J = 7.1 Hz, 2H), 2.99–2.84 (m, 2H), 2.84–2.73 (m, 1H), 1.91–1.84 (m, 2H), 1.73–1.58 (m, 2H), 1.28–1.26 (m, 3H). HRMS m/z [M + H] $^+$ for C₃₂H₂₉F₃NO₄ calculated 548.2049, found 548.2042.

Ethyl 4-(4-(3-((2-(Dimethylamino)-2-oxoethoxy)carbonyl)-6-(4-(trifluoromethyl)phenyl)naphthalen-1-yl)phenyl)piperidine-1-carboxylate (62).—To a solution of **61** (667 mg, 1.22 mmol) and Cs₂CO₃ (795 mg, 2.44 mmol) in DMF (20 mL) under argon atmosphere was added 2-chloro-*N,N*-dimethylacetamide (151 μ L, 178 mg, 1.464 mmol). The reaction mixture was stirred at rt overnight. The reaction mixture was partitioned between ethyl acetate (20 mL) and water (20 mL), and the aqueous phase was extracted with ethyl acetate (2 \times 20 mL). The combined organic layers were dried over Na₂SO₄, filtered, and concentrated under pressure. The residue was purified by silica gel chromatography (hexane/ethyl acetate = 70:30 \rightarrow 35:65) to afford compound **62** (480 mg, 62%) as a white solid: $^1\text{H NMR}$ (400 MHz, CDCl₃) δ 8.74 (s, 1H), 8.19 (d, J = 1.9 Hz, 1H), 8.07 (d, J = 1.7 Hz, 1H), 8.02 (d, J = 8.8 Hz, 1H), 7.82–7.69 (m, 5H), 7.44 (d, J = 7.8 Hz, 2H), 7.32 (d, J = 7.8 Hz, 2H), 5.01 (s, 2H), 4.40–4.26 (m, 2H), 4.15 (q, J = 7.1 Hz, 2H), 3.04 (s, 3H), 2.99 (s, 3H), 2.96–2.83 (m, 2H), 2.80–2.70 (m, 1H), 1.96–1.88 (m, 2H), 1.77–1.64 (m, 2H), 1.31–1.24 (m, 3H). $^{13}\text{C NMR}$ (126 MHz, CDCl₃) δ 166.41, 166.35, 155.75, 145.32, 144.00, 140.60, 137.86, 137.79, 133.62, 133.40, 131.42, 130.28, 128.19, 127.78, 127.20, 126.99, 126.04, 62.11, 61.45, 44.61, 42.47, 36.07, 35.76, 33.31, 14.89. HRMS m/z [M + H] $^+$ for C₃₆H₃₆F₃N₂O₅ calculated 633.2576, found 633.2574.

Characterization of Lipophilicity.

pION Solubility Tests: pION Buffer and Blank Buffer Preparation.—pION solubility tests were performed with pION system solution (pION, Inc., Billerica, MA, P/

N 110151). pH 4.0 and 7.4 pION buffers were prepared by adding 2.5 mL of pION system solution to 97.5 mL of Milli-Q water and adjusting the pH to 4.0 and 7.4 with 0.5 N NaOH, respectively. Blank buffers were prepared by mixing 15 mL of pION buffers (pH 4.0 and 7.4) with 14 mL of *n*-propanol.

Control and Sample UV Plate Preparation.—All ligands were stored as 5 mM stock solutions in DMSO. 3 μL of each ligand stock solution (including DMSO control) was added to 300 μL of pH 4.0 and 7.4 pION buffers, mixed, and incubated for 20 h. The undissolved compound particles were removed by centrifuge at 14,000 rpm for 20 min. 100 μL of supernatant was added to a 96-well plate containing 100 μL of *n*-propanol and mixed well with a pipette.

Reference UV Plate Preparation.—4 μL of each ligand stock solution was added to 76 μL of *n*-propanol. 10 μL of resulting solution was added to 290 μL of blank buffer, mixed, and incubated for 20 h. 200 μL of the reference solution with a final concentration of ligand as 8.33 μM was transferred to a 96-well plate.

UV Absorption Tests.—The Greiner UV-Star 96-well plates have low UV absorption background and excellent resistance to general organic solvents. The UV absorption of control (A_{control}), ligands (A_{ligand}), and references ($A_{\text{reference}}$) were collected in triplicate at the ligands' maximum absorption at 270 nm.

Solubility Calculation.— $\text{Solubility}_{(\text{ligand})} = 2 \times \text{average}(A_{\text{sample}} - A_{\text{control}}) / \text{average}(A_{\text{reference}} - A_{\text{control}}) \times 8.33 \mu\text{M} = 2 \times \text{average}(A_{\text{sample}} - A_{\text{control}}) / \text{average}(A_{\text{reference}} - A_{\text{control}}) \times 8.33 \times M \times 10^{-3} \mu\text{g/mL}$.

Relative Lipophilicities of Analogues of 1 Compared to 1.—All ligands were stored as 250 μM stock solutions in DMSO. HPLC-based measurements of relative lipophilicities of analogues of **1** compared to **1** were carried out with an Agilent Eclipse XDB-C18(4.6 mm \times 250 mm, 5 μm) and a 20 min gradient of 10 to 100% acetonitrile in 10 mM triethylammonium acetate with a flow rate as 1.0 mL/min.

The HPLC-based lipophilicity of each ligand was calculated from a calibration curve using five standards and plotting their respective measured retention factor (k) versus reported $\text{Log } D_{7.4}$ from the literature (Table S2, Figure S3). The correlation of $\text{Log } D_{7.4}$ to k has a correlation coefficient r^2 of 0.986. The lipophilicities $\text{Log } D_{7.4}$ of modified piperidine analogues of piperidine **1** are exhibited in Table 1 and Figure S4.

Mouse Models of Mechano-Allodynia and Protease-Induced Asthma.

Mouse mechano-allodynia in Hsd:ICR (CD-1) outbred adult males (20–30 g, Envigo, Indianapolis, IN) was determined as described.¹⁰ The drugs were administered i.p. on the day of peak pain (7 days, post-surgery). The methods conformed to the guidelines of the International Association for the Study of Pain and the National Institutes of Health and were approved by the Institutional Animal Care and Use Committee (IACUC) of St. Louis University.

Compound **15** and one antagonist double prodrug **50** were tested in mice (C57BL/6J, Jackson Laboratory, Bar Harbor, ME) displaying protease-induced asthma.⁶ There were two sensitizations, one week apart, consisting of oropharyngeal instillation of 50 μg of LPS-free ovalbumin (OVA, Worthington Biomedical, CA) and 20 μg of *Aspergillus oryzae* (Sigma-Aldrich, St. Louis, MO) in 50 μL of phosphate-buffered saline (PBS). The antagonist injection was performed on the day of ovalbumin challenge (day 14 post-initial sensitization using ovalbumin/*Aspergillus*), intraperitoneally at a dose of 10 mg/kg with 10 mL/kg vehicle (10% DMSO, 30% PEG-400, 60% water). Following 30 min, the mice inhaled 1% OVA aerosol in PBS for 1 h. 48 h later, BALF was collected, and the inflammatory cells were counted. The animal protocol was approved by the NIEHS IACUC (Research Triangle Park, NC).

Supplementary Material

Refer to Web version on PubMed Central for supplementary material.

ACKNOWLEDGMENTS

The authors thank the NIH, National Institute of Diabetes and Digestive and Kidney Diseases Intramural Research Program (ZIADK031116) and Kantum Pharma, Inc. (Concord, NH) for support through NIDDK CRADA 17-0824. They also thank Tocris (Bristol, U.K.) for the gift of reactive fluorophore intermediates (JaneliaFluor dyes), and Dr. Bryan L. Roth (Univ. North Carolina at Chapel Hill) and National Institute of Mental Health's Psychoactive Drug Screening Program (Contract # HHSN-271-2008-00025-C) for screening data.

ABBREVIATIONS USED

ADME	absorption, distribution, metabolism, and excretion
AAR/TTA	area at risk/total area of left ventricle
BAL	bronchoalveolar lavage
CCI	chronic constriction injury
CHO	Chinese hamster ovary
CXCL	chemokine (C-X-C motif) ligand
DCM	dichloromethane
DMAP	4-dimethylaminopyridine
DMF	<i>N,N</i> -dimethylformamide
IF	infarct size
IL	interleukin
I/R	ischemia/reperfusion
MI	myocardial infarction
PDSP	NIMH Psychoactive Drug Screening Program

PWT	paw withdrawal threshold
SAR	structure–activity relationship
SLC	solute carrier
UDPG	uridine-5′-diphosphoglucose
TEA	triethylamine
TEAA	triethylammonium acetate
TFA	trifluoroacetic acid
THF	tetrahydrofuran

REFERENCES

- (1). Klaver D; Thurnher M Control of macrophage inflammation by P2Y purinergic receptors. *Cells* 2021, 10, 1098. [PubMed: 34064383]
- (2). Arase T; Uchida H; Kajitani T; Ono M; Tamaki K; Oda H; Nishikawa S; Kagami M; Nagashima T; Masuda H; Asada H; Yoshimura Y; Maruyama T The UDP-glucose receptor P2RY₁₄ triggers innate mucosal immunity in the female reproductive tract by inducing IL-8. *J. Immunol* 2009, 182, 7074–7084. [PubMed: 19454705]
- (3). Müller T; Bayer H; Myrtek D; Ferrari D; Sorichter S; Ziegenhagen MW; Zissel G; Virchow JC Jr.; Luttmann W; Norgauer J; Di Virgilio F; Idzko M The P2Y₁₄ receptor of airway epithelial cells: Coupling to intracellular Ca²⁺ and IL-8 secretion. *Am. J. Respir. Cell Mol. Biol* 2005, 33, 601–609. [PubMed: 16109883]
- (4). Battistone MA; Mendelsohn AC; Spallanzani RG; Allegretti AS; Liberman RN; Sesma J; Kalim S; Wall SM; Bonventre JV; Lazarowski ER; Brown D; Breton S Proinflammatory P2Y₁₄ receptor inhibition protects against ischemic acute kidney injury in mice. *J. Clin. Invest* 2020, 130, 3734–3749. [PubMed: 32287042]
- (5). Wen Z; Salmaso V; Jung Y-H; Phung NB; Gopinath V; Shah Q; Patterson AT; Randle JCR; Chen Z; Salvemini D; Lieberman DI; Whitehead GS; Karcz TP; Cook DN; Jacobson KA Bridged piperidine analogues of a high affinity naphthalene-based P2Y₁₄R antagonist. *J. Med. Chem* 2022, 65, 3434–3459. [PubMed: 35113556]
- (6). Karcz TP; Whitehead GS; Nakano K; Nakano H; Grimm SA; Williams JG; Deterding LJ; Jacobson KA; Cook DN UDP-glucose and P2Y₁₄ receptor amplify allergen-induced airway eosinophilia. *J. Clin. Invest* 2021, 131, No. e140709.
- (7). Ko H; Das A; Carter RL; Fricks IP; Zhou Y; Ivanov AA; Melman A; Joshi BV; Kovác P; Hajduch J; Kirk KL; Harden TK; Jacobson KA Molecular recognition in the P2Y₁₄ receptor: Probing the structurally permissive terminal sugar moiety of uridine-5′-diphosphoglucose. *Bioorg. Med. Chem* 2009, 17, 5298–5311. [PubMed: 19502066]
- (8). Hamel M; Henault M; Hyjazie H; Morin N; Bayly C; Skorey K; Therien AG; Mancini J; Brideau C; Kargman S Discovery of novel P2Y₁₄ agonist and antagonist using conventional and nonconventional methods. *SLAS Discovery* 2011, 16, 1098–1105.
- (9). Jain S; Pydi SP; Jung YH; Scortichini M; Kesner EL; Karcz TP; Cook DN; Gavrilova O; Wess J; Jacobson KA Adipocyte P2Y₁₄ receptors play a key role in regulating whole-body glucose and lipid homeostasis. *JCI Insight* 2021, 6, No. e146577.
- (10). Mufti F; Jung YH; Giancotti LA; Yu J; Chen Z; Phung NB; Jacobson KA; Salvemini D P2Y₁₄ receptor antagonists reverse chronic neuropathic pain in a mouse model. *ACS Med. Chem. Lett* 2020, 11, 1281–1286. [PubMed: 32551012]
- (11). Patriiti Cram J; Wu J; Coover RA; Rizvi TA; Chaney KE; Ravindran R; Cancelas JA; Spinner RJ; Ratner N P2RY₁₄ cAMP signaling regulates Schwann cell precursor self-renewal, proliferation, and nerve tumor initiation in a mouse model of neurofibromatosis. *eLife* 2022, 11, No. e73511.

- (12). Liu C; Zhou M; Jiang W; Ye S; Tian S; Jiang C; Hao K; Li H; Hu Q GPR105-targeted therapy promotes gout resolution as a switch between NETosis and apoptosis of neutrophils. *Front. Immunol* 2022, 13, No. 870183.
- (13). Xu J; Morinaga H; Oh D; Li P; Chen A; Talukdar S; Mamane Y; Mancini JA; Nawrocki AR; Lazarowski E; Olefsky JM; Kim JJ GPR105 ablation prevents inflammation and improves insulin sensitivity in mice with diet-induced obesity. *J. Immunol* 2012, 189, 1992–1999. [PubMed: 22778393]
- (14). Khalafalla FG; Kayani W; Kassab A; Ilves K; Monsanto MM; Alvarez R; Chavarria M Jr; Norman B; Dembitsky WP; Sussman MA Empowering human cardiac progenitor cells by P2Y₁₄ nucleotide receptor overexpression. *J. Physiol* 2017, 595, 7135–7148. [PubMed: 28980705]
- (15). Belley M; Deschenes D; Fortin R; Fournier J-F; Gagne S; Gareau Y; Gauthier JY; Li L; Robichaud J; Therien M; Tranmer GK; Wang Z Substituted 2-naphthoic acids as antagonists of GPR105 activity. WO2009070873A1, June 11, 2009.
- (16). Barrett MO; Sesma JI; Ball CB; Jayasekara PS; Jacobson KA; Lazarowski ER; Harden TK A selective high affinity antagonist of the P2Y₁₄ receptor inhibits UDP-glucose-stimulated chemotaxis of human neutrophils. *Mol. Pharmacol* 2013, 84, 41–49. [PubMed: 23592514]
- (17). Jung YH; Yu J; Wen Z; Salmaso V; Phung NB; Karcz T; Chen Z; Duca S; Bennett JM; Dudas S; Cook DN; Salvemini D; Gao ZG; Jacobson KA Exploration of alternative scaffolds for P2Y₁₄ receptor antagonists containing a biaryl core. *J. Med. Chem* 2020, 63, 9563–9589. [PubMed: 32787142]
- (18). Robichaud J; Fournier J-F; Gagné S; Gauthier JY; Hamel M; Han Y; Hénault M; Kargman S; Levesque JF; Mamane Y; Mancini J; Morin N; Mulrooney E; Wu J; Black WC Applying the pro-drug approach to afford highly bioavailable antagonists of P2Y₁₄. *Bioorg. Med. Chem. Lett* 2011, 21, 4366–4368. [PubMed: 21689930]
- (19). Jung YH; Salmaso V; Wen Z; Bennett JM; Phung NB; Lieberman DI; Gopinath V; Randle JCR; Chen Z; Salvemini D; Karcz TP; Cook DN; Jacobson KA Structure-activity relationship of heterocyclic P2Y₁₄ receptor antagonists: Removal of the zwitterionic character with piperidine bioisosteres. *J. Med. Chem* 2021, 64, 5099–5122. [PubMed: 33787273]
- (20). Zhou M; Wang W; Wang Z; Wang Y; Zhu Y; Lin Z; Tian S; Huang Y; Hu Q; Li H Discovery and computational studies of 2-phenyl-benzoxazole acetamide derivatives as promising P2Y₁₄R antagonists with anti-gout potential. *Eur. J. Med. Chem* 2022, 227, No. 113933.
- (21). Wang YH; Zhou MZ; Ye T; Wang PP; Lu R; Wang YL; Liu CX; Xiao W; Li JY; Meng ZB; Xu LL; Hu QH; Jiang C Discovery of a series of 5-amide-1H-pyrazole-3-carboxyl derivatives as potent P2Y₁₄R antagonists with anti-inflammatory characters. *J. Med. Chem* 2022, 65, 15967–15990. [PubMed: 36394994]
- (22). Kalgutkar AS; Driscoll JP Is there enough evidence to classify cycloalkyl amine substituents as structural alerts? *Biochem. Pharmacol* 2020, 174, No. 113796.
- (23). van der Kolk MR; Jansen MACH; Rutjes FPJT; Blanco-Ania D Cyclobutanes in small molecule drug candidates. *ChemMedChem* 2022, 17, No. e202200020.
- (24). Shearer J; Castro JL; Lawson ADG; MacCoss M; Taylor RD Rings in clinical trials and drugs: Present and future. *J. Med. Chem* 2022, 65, 8699–8712. [PubMed: 35730680]
- (25). Segall MD Multi-parameter optimization: identifying high quality compounds with a balance of properties. *Curr. Pharm. Des* 2012, 18, 1292–1310. [PubMed: 22316157]
- (26). Yu J; Ciancetta A; Dudas S; Duca S; Lottemoser J; Jacobson KA Structure-guided modification of heterocyclic antagonists of the P2Y₁₄ receptor. *J. Med. Chem* 2018, 61, 4860–4882. [PubMed: 29767967]
- (27). Ganiu MO; Cleveland AH; Paul JL; Kartika R Triphosgene and DMAP as mild reagents for chemoselective dehydration of tertiary alcohols. *Org. Lett* 2019, 21, 5611–5615. [PubMed: 31251637]
- (28). Mandal PK; McMurray JS Pd–C-induced catalytic transfer hydrogenation with triethylsilane. *J. Org. Chem* 2007, 72, 6599–6601. [PubMed: 17630799]
- (29). Ghosh AK; Brindisi M Organic carbamates in drug design and medicinal chemistry. *J. Med. Chem* 2015, 58, 2895–2940. [PubMed: 25565044]

- (30). Kiselev E; Barrett M; Katritch V; Paoletta S; Weitzer CD; Brown KA; Hammes E; Hammes E; Yin AL; Yin AL; Zhao Q; Zhao Q; Stevens RC; Stevens RC; Harden TK; Harden TK; Jacobson KA Exploring a 2-naphthoic acid template for the structure-based design of P2Y₁₄ receptor antagonist molecular probes. *ACS Chem. Biol* 2014, 9, 2833–2842. [PubMed: 25299434]
- (31). Cheng Y; Prusoff WH Relationship between the inhibition constant (K₁) and the concentration of inhibitor which causes 50 per cent inhibition (I₅₀) of an enzymatic reaction. *Biochem. Pharmacol* 1973, 22, 3099–3108. [PubMed: 4202581]
- (32). Grimm JB; Muthusamy AK; Liang Y; Brown TA; Lemon WC; Patel R; Lu R; Macklin JJ; Keller PJ; Ji N; Lavis LD A general method to fine-tune fluorophores for live-cell and in vivo imaging. *Nat. Methods* 2017, 14, 987–994. [PubMed: 28869757]
- (33). Abdelshaheed MM; Fawzy IM; El-Subbagh HI; Youssef KM Piperidine nucleus in the field of drug discovery. *Future J. Pharm. Sci* 2021, 7, No. 188.
- (34). Ratni H; Baumann K; Bellotti P; Cook XA; Green LG; Luebbers T; Reutlinger M; Stepan AF; Vifian W Phenyl bioisosteres in medicinal chemistry: discovery of novel γ -secretase modulators as a potential treatment for Alzheimer's disease. *RSC Med. Chem* 2021, 12, 758–766. [PubMed: 34124674]
- (35). Sheffler DJ; Nedelcovych MT; Williams R; Turner SC; Duerk BB; Robbins MR; Jadhav SB; Niswender CM; Jones CK; Conn PJ; Daniels RN; Lindsley CW Novel GlyT1 inhibitor chemotypes by scaffold hopping. Part 2: development of a [3.3.0]-based series and other piperidine bioisosteres. *Bioorg. Med. Chem. Lett* 2014, 24, 1062–1066. [PubMed: 24462664]
- (36). Carreira EM; Fessard TC Four-membered ring-containing spirocycles: Synthetic strategies and opportunities. *Chem. Rev* 2014, 114, 8257–8322. [PubMed: 25003801]
- (37). Burkhard JA; Wagner B; Fischer H; Schuler F; Müller K; Carreira EM Synthesis of azaspirocycles and their evaluation in drug discovery. *Angew. Chem., Int. Ed* 2010, 49, 3524–3527.
- (38). Ouvry G Recent applications of seven-membered rings in drug design. *Bioorg. Med. Chem* 2022, 57, No. 116650.
- (39). Besnard J; Ruda GF; Setola V; Abecassis K; Rodriguiz RM; Huang XP; Norval S; Sassano MF; Shin AI; Webster LA; Simeons FR; Stojanovski L; Prat A; Seidah NG; Constam DB; Bickerton GR; Read KD; Wetsel WC; Gilbert IH; Roth BL; Hopkins AL Automated design of ligands to polypharmacological profiles. *Nature* 2012, 492, 215–220. [PubMed: 23235874]
- (40). Valkó K Application of high-performance liquid chromatography based measurements of lipophilicity to model biological distribution. *J. Chromatogr. A* 2004, 1037, 299–310. [PubMed: 15214672]
- (41). Bennett GJ; Xie YK A peripheral mononeuropathy in rat that produces disorders of pain sensation like those seen in man. *Pain* 1988, 33, 87–107. [PubMed: 2837713]
- (42). Kuhn B; Mohr P; Stahl M Intramolecular hydrogen bonding in medicinal chemistry. *J. Med. Chem* 2010, 53, 2601–2611. [PubMed: 20175530]
- (43). Ashwood VA; Field MJ; Horwell DC; Julien-Larose C; Lewthwaite RA; McCleary S; Pritchard MC; Raphy J; Singh L Utilization of an intramolecular hydrogen bond to increase the CNS penetration of an NK₁ receptor antagonist. *J. Med. Chem* 2001, 44, 2276–2285. [PubMed: 11428921]
- (44). Duncan SE; Gao S; Sarhene M; Coffie JW; Linhua D; Bao X; Jing Z; Li S; Guo R; Su J; Fan G Macrophage activities in myocardial infarction and heart failure. *Cardiol. Res. Pract* 2020, 2020, 1–16.
- (45). Bohl S; Medway DJ; Schulz-Menger J; Schneider JE; Neubauer S; Lygate CA Refined approach for quantification of in vivo ischemia and reperfusion injury in the mouse heart. *Am. J. Physiol. Heart Circ. Physiol* 2009, 297, H2054–H2058. [PubMed: 19820193]
- (46). Liu W; Cronin C; Cao Z; Wang C; Ruan J; Pulikkot S; Hall A; Sun H; Groisman A; Chen Y; Vella AT; Hu L; Liang BT; Fan Z Nexinhib20 inhibits neutrophil adhesion and β 2 integrin activation by antagonizing Rac-1-Guanosine 5'-Triphosphate Interaction. *J. Immunol* 2022, 209, 1574–1585. [PubMed: 36165184]
- (47). Qian C; Wu Z; Sun R; Yu H; Zeng J; Rao Y; Li Y Localization, proteomics, and metabolite profiling reveal a putative vesicular transporter for UDP-glucose. *eLife* 2021, 10, No. e65417.

- (48). Breton S; Battistone MA Unexpected participation of intercalated cells in renal inflammation and acute kidney injury. *Clinical Practice: Mini-Review. Nephron* 2021, DOI: [10.1159/000519265](https://doi.org/10.1159/000519265).
- (49). Leeson PD; Bento AP; Gaulton A; Hersey A; Manners EJ; Radoux CJ; Leach AR Target-based evaluation of “drug-like” properties and ligand efficiencies. *J. Med. Chem* 2021, 64, 7210–7230. [PubMed: 33983732]

Author Manuscript

Author Manuscript

Author Manuscript

Author Manuscript

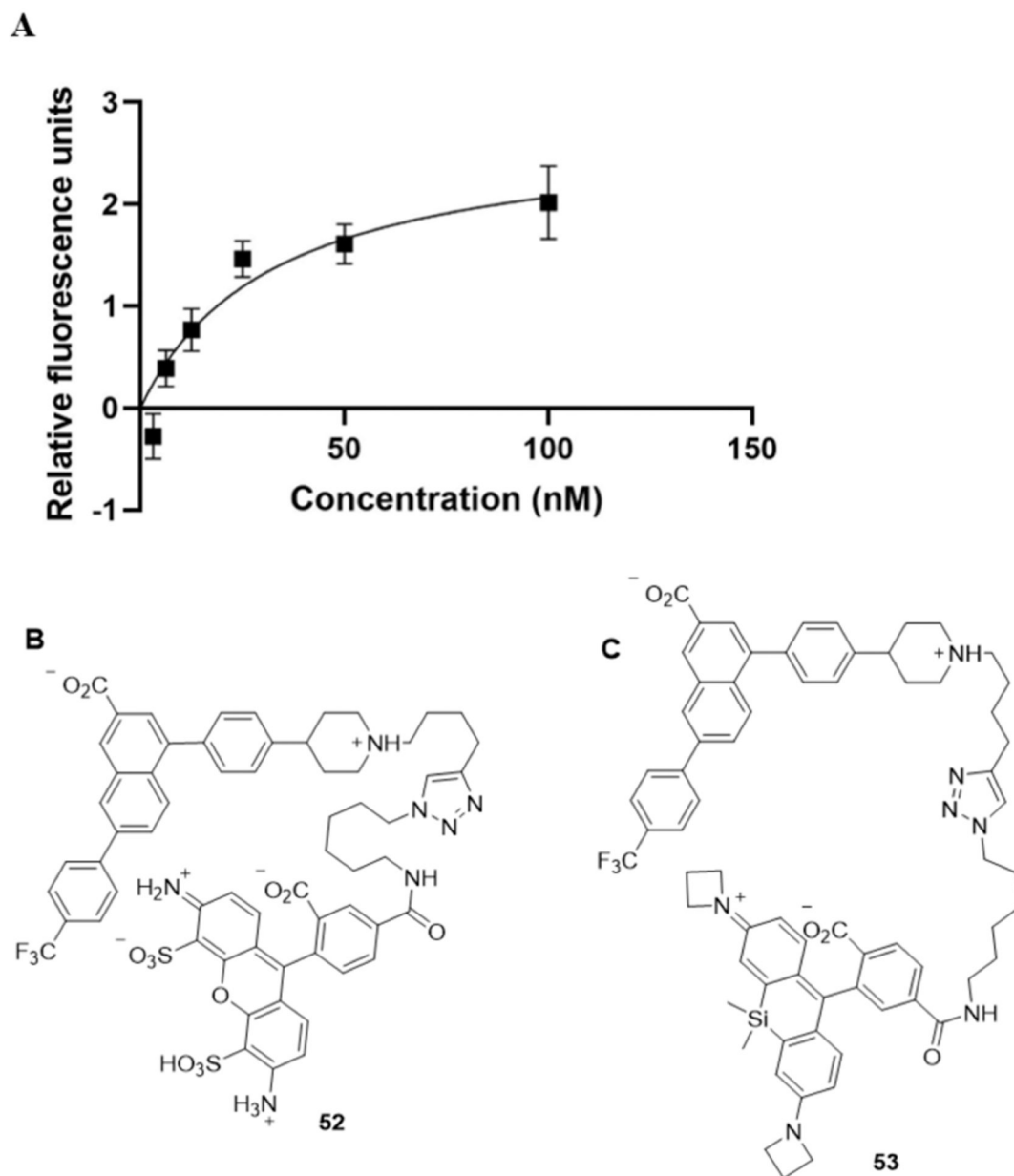


Figure 1. Representative saturation curve (A) for specific binding of **52** (B) to the hP2Y₁₄R in hP2Y₁₄R-expressing CHO cells, as determined using flow cytometry. (C) Structure of the newly prepared fluorescent conjugate **53** of JaneliaFluor 646³² with the same pharmacophore as **52**.

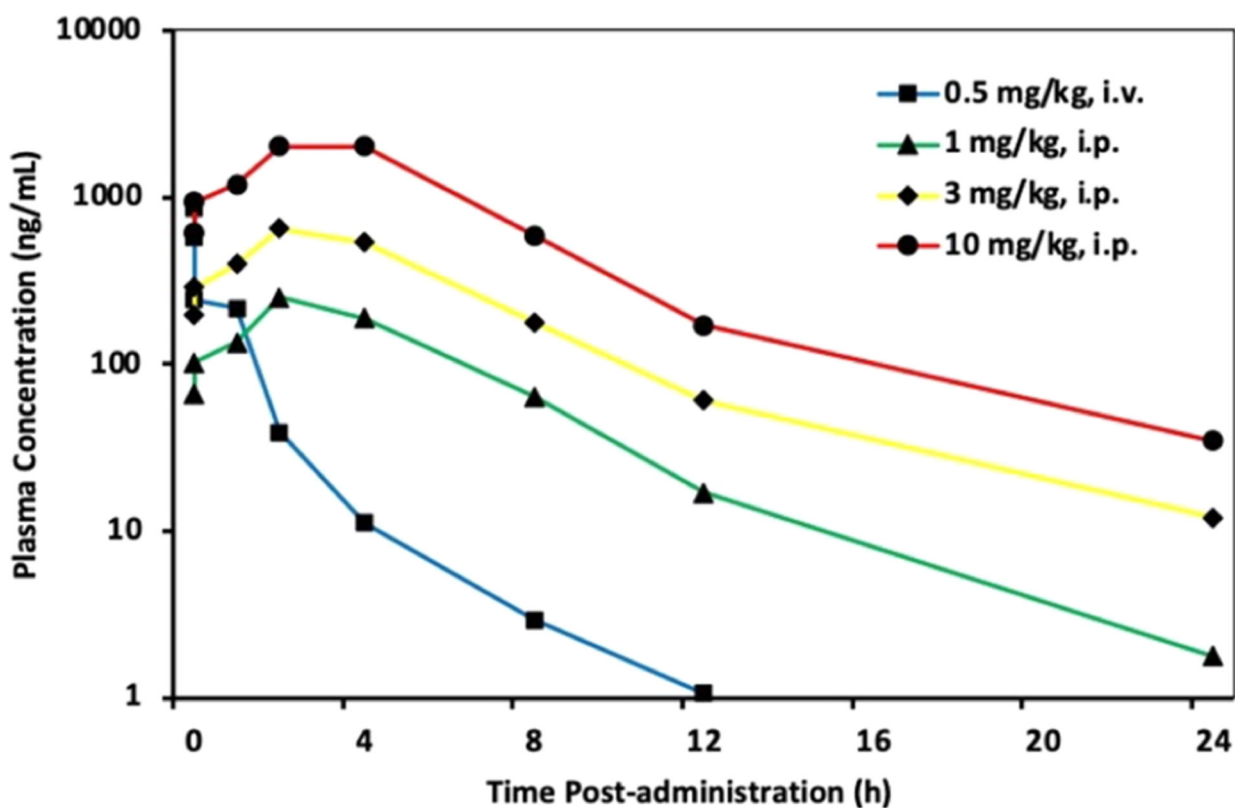


Figure 2. Plasma levels of compound **15** following administration to male Wistar rats. Pharmacokinetic (PK) parameters and conditions are shown in Table S3A,C,D (Supporting Information). Half-life values (i.p. dose, h) were: 1.0 mg/kg, 3.01; 3.0 mg/kg, 4.32; 10.0 mg/kg, 4.15. Half-life at 0.5 mg/kg, i.v. was 2.36 h. Maximal plasma concentration (mg/kg i.p., μM): were: 1.0, 0.50; 3.0, 1.3; 10.0, 4.0.

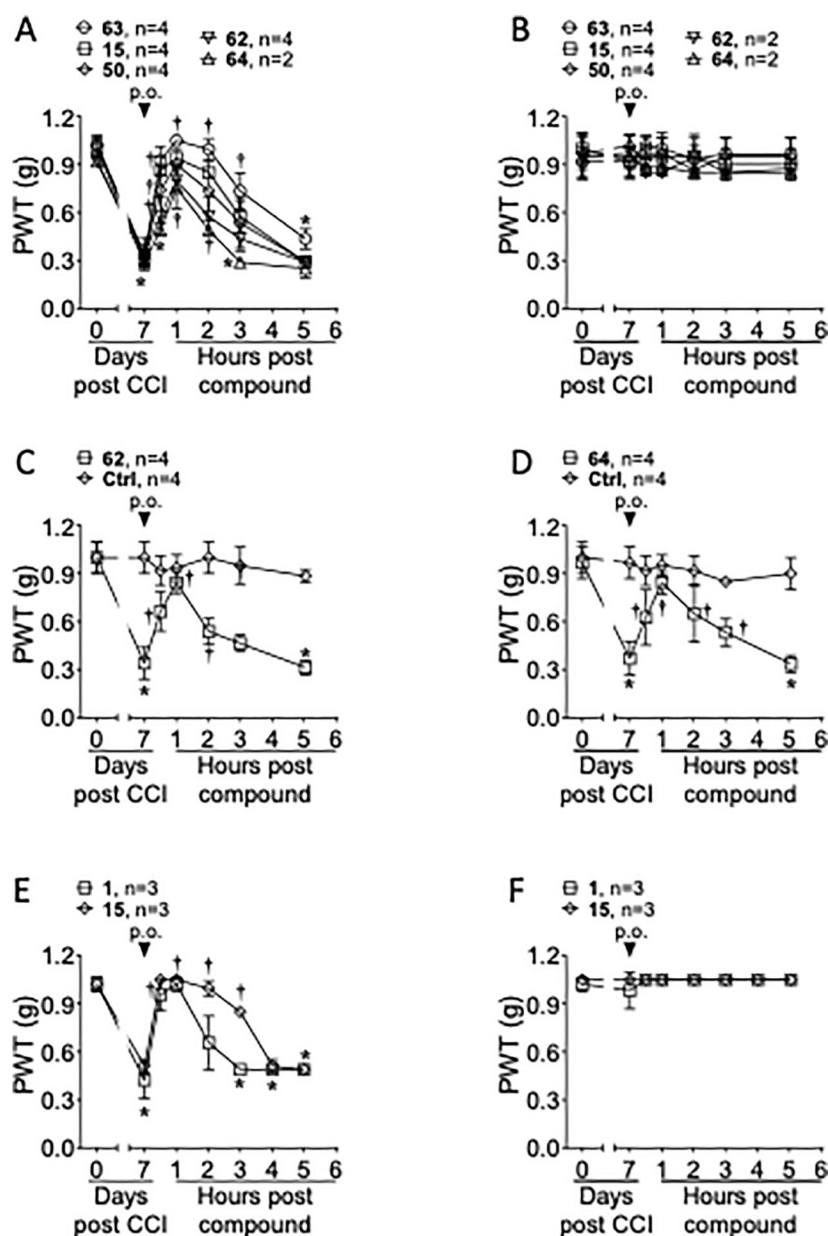


Figure 3. Representative time and dose dependence for reversal of established neuropathic pain in adult male mice by five newly synthesized P2Y₁₄R antagonists and reference compound **1**. The drugs were injected 7 days post-sciatic nerve constriction. The paw withdrawal threshold (PWT) was determined using von Frey filaments applied to the postsurgical hindpaw.⁴¹ (A–D) Single injection (10 μ mol/kg, p.o.) of a P2Y₁₄ R antagonist (active drug **15** or prodrugs **50** and **62–64**) reversed the mechano-allodynia on the ipsilateral, nerve-injured hindpaw. (E, F) Reference antagonist **1** was compared to the potent antagonist **15**, with both administered by oral gavage. A single p.o. administration (10 μ mol/kg) of **1** or **15** reversed the mechano-allodynia. For all experiments, the drug injection had no effect on the contralateral hindpaw (B, F). Data were analyzed by twoway analysis of variance

(ANOVA) with Dunnett's comparisons, * $P < 0.05$ versus day 0 and † $P < 0.05$ versus day 7. Data represent the mean \pm SD. The vehicle used for the oral dosing consisted of 5% dimethyl sulfoxide (DMSO) + 10% (5% Kolliphor HS 15:DMSO, 5:95 by volume) in 0.5% methyl cellulose (0.2 mL dose). The vehicle used for the i.p. injection: 10% (5% Kolliphor HS 15:DMSO, 5:95 by volume) in saline (0.2 mL dose). Results with other antagonists (**11**, **15**, and **16**; i.p.) in the mouse CCI model are shown in Figure S8 (Supporting Information).

Author Manuscript

Author Manuscript

Author Manuscript

Author Manuscript

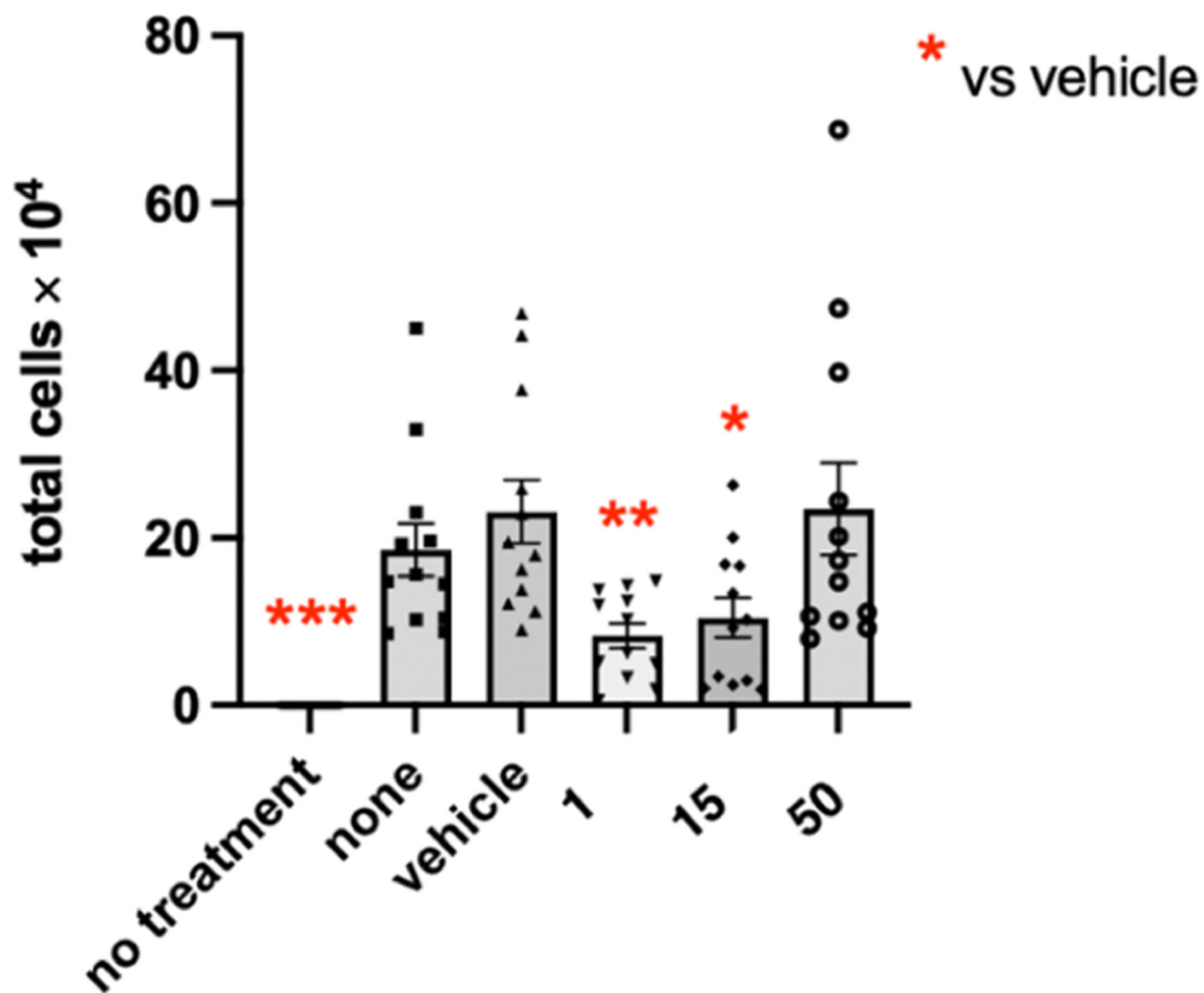
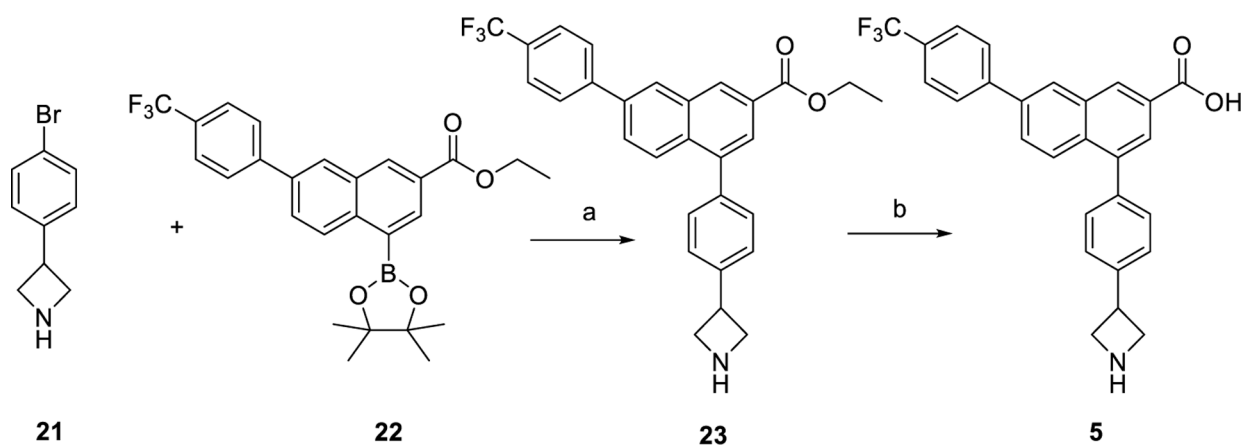
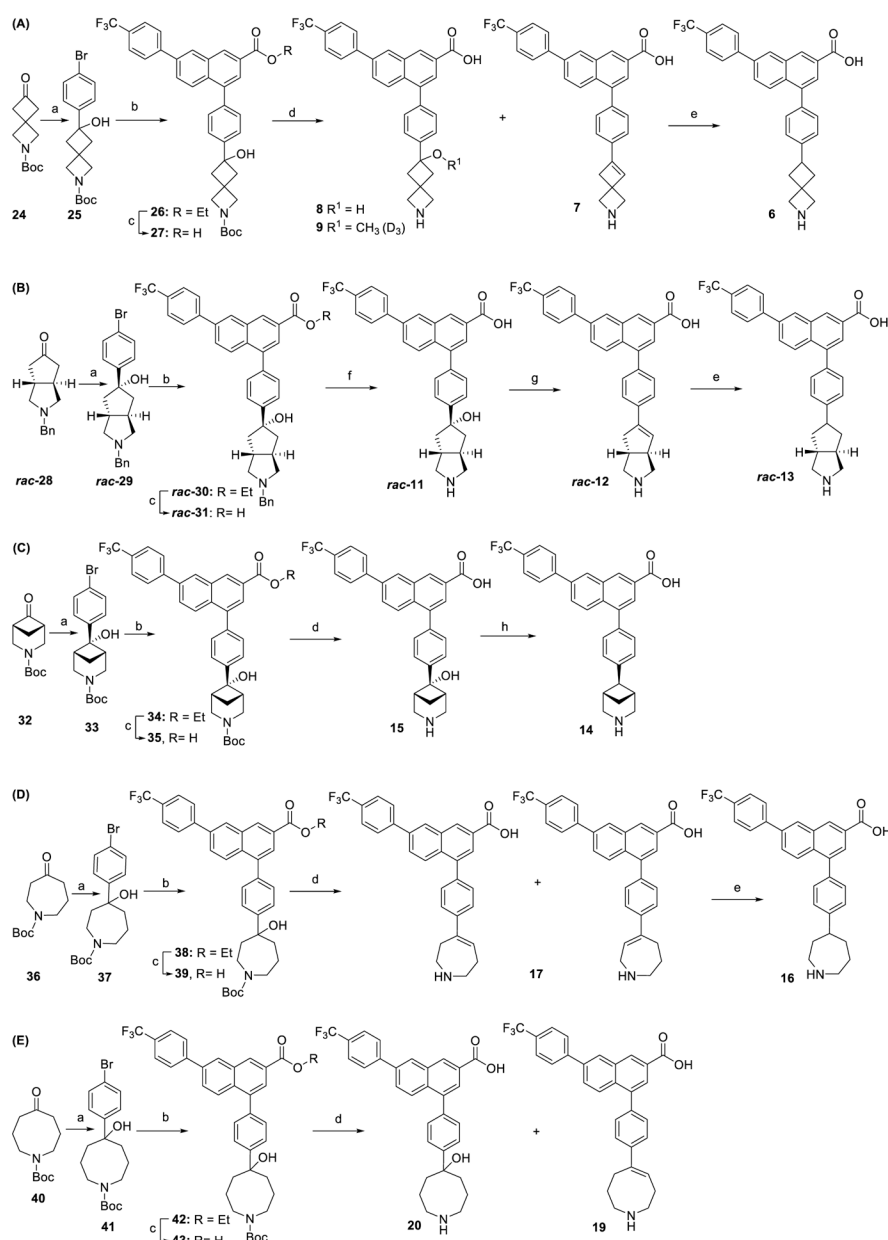


Figure 4. Ability of compound **15**, but not its double (ester and carbamate) prodrug **50**, and the reference antagonist **1** to reduce airway eosinophilia in a protease-mediated mouse model of allergic asthma. Results with other BAL fluid cells are shown in Figure S7 (Supporting Information).

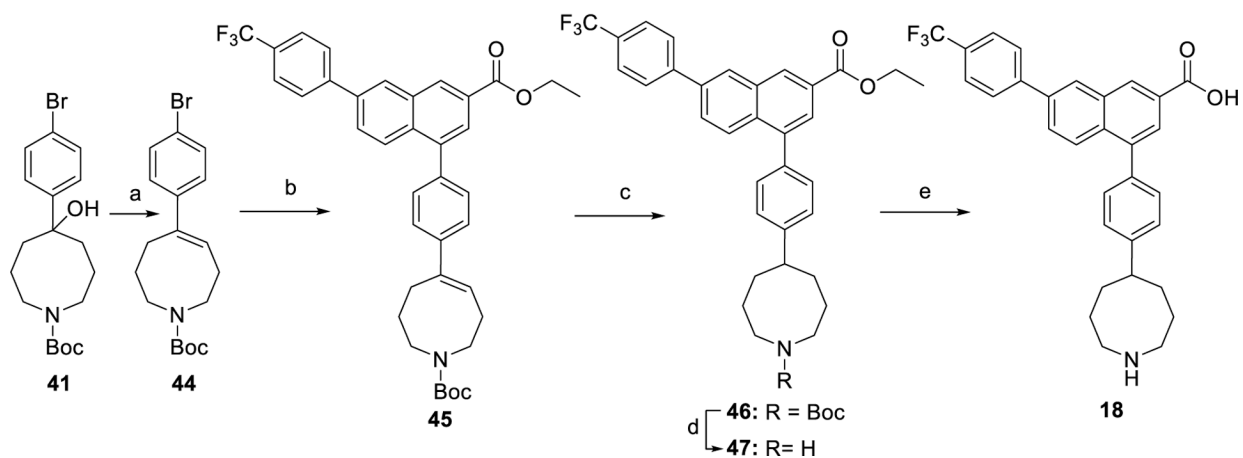
**Scheme 1.**Synthesis of an Analogue of 1 Containing Azetidines^a

^aReagents and conditions: (a) Na₂CO₃, Pd(PPh₃)₄, 1,2-dimethoxyethane (DME)-H₂O (4:1), 80 °C, overnight, 57%; (b) LiOH, tetrahydrofuran (THF)-MeOH-H₂O (3:1:1), rt, 3 h, 47%.

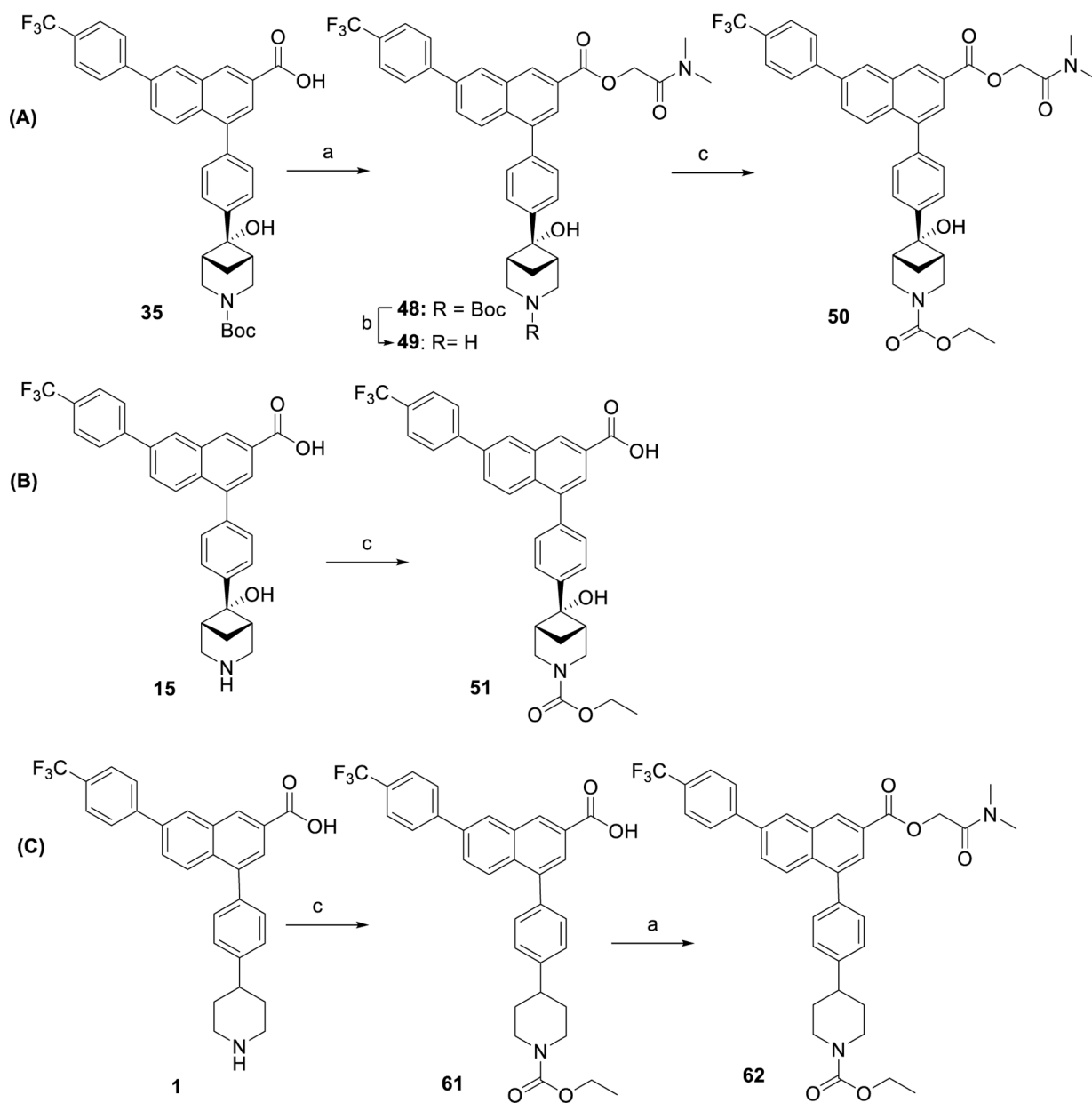
**Scheme 2.**

Preparation of Analogues of **1** with 2-Azasp[3.3]heptane (A), Octahydrocyclopenta[*c*]pyrrole (B), 3-Azabicyclo[3.1.1]heptane (C), 1-Azacycloheptane (D), and Azocane (E) Moieties^a

^aReagents and conditions: (a) 4-bromophenylmagnesium bromide (in situ generated: dibromobenzene, magnesium, THF, sonication, rt, 2 h), THF, 0 °C, 4 h, 39–81%; (b) boronic acid pinacol ester **22**, Na₂CO₃, Pd(PPh₃)₄, DME-H₂O (4:1), 85 °C, overnight, 57–93%; (c) LiOH, THF MeOH-H₂O (3:1:1), rt, 3 h, quantitative; (d) trifluoroacetic acid (TFA), dichloromethane (DCM), rt, 1 h, 18–52%; (e) H₂, Pd/C, *N,N*-dimethylformamide (DMF), 3 h, 22–51%; (f) H₂, Pd/C, DMF, 5 h, 35% overall yield from **30**; (g) TFA, 90 °C, 2 h, 33% overall yield from **31**; (h) NaBH₄, THF, H₂SO₄, rt, 30 min, 11%.

**Scheme 3.**Preparation of Azocane Analogue 18 Using Alternative Synthetic Strategies^a

^aReagents and conditions: (a) triphosgene, DMAP, DCM, rt, 2 h, quantitative; (b) boronic acid pinacol ester **22**, Na₂CO₃, Pd(PPh₃)₄, DME-H₂O (4:1), 85 °C, overnight, quantitative; (c) Et₃SiH, 10% Pd/C, MeOH/THF = 1:5, rt, 30 min, quantitative; (d) TFA, THF, rt, 20 min, quantitative; (e) LiOH, THF-MeOH-H₂O (3:1:1), rt, 2 h, overall yield 54% from **45**.

**Scheme 4.**

Preparation of Double (A) and Mono (A and B) Prodrugs of 15 (i.e., 49–51) as well as Double Prodrug 62 of 1 (C)^a

^aReagents and conditions: (a) 2-chloro-*N,N*-dimethylacetamide, Cs₂CO₃, DMF, rt, overnight, 56%-quantitative; (b) TFA, DCM, rt, 1 h, 59%; (c) ethyl chloroformate, *N,N*-diisopropylethylamine, DMF, rt, overnight, 17–62%.

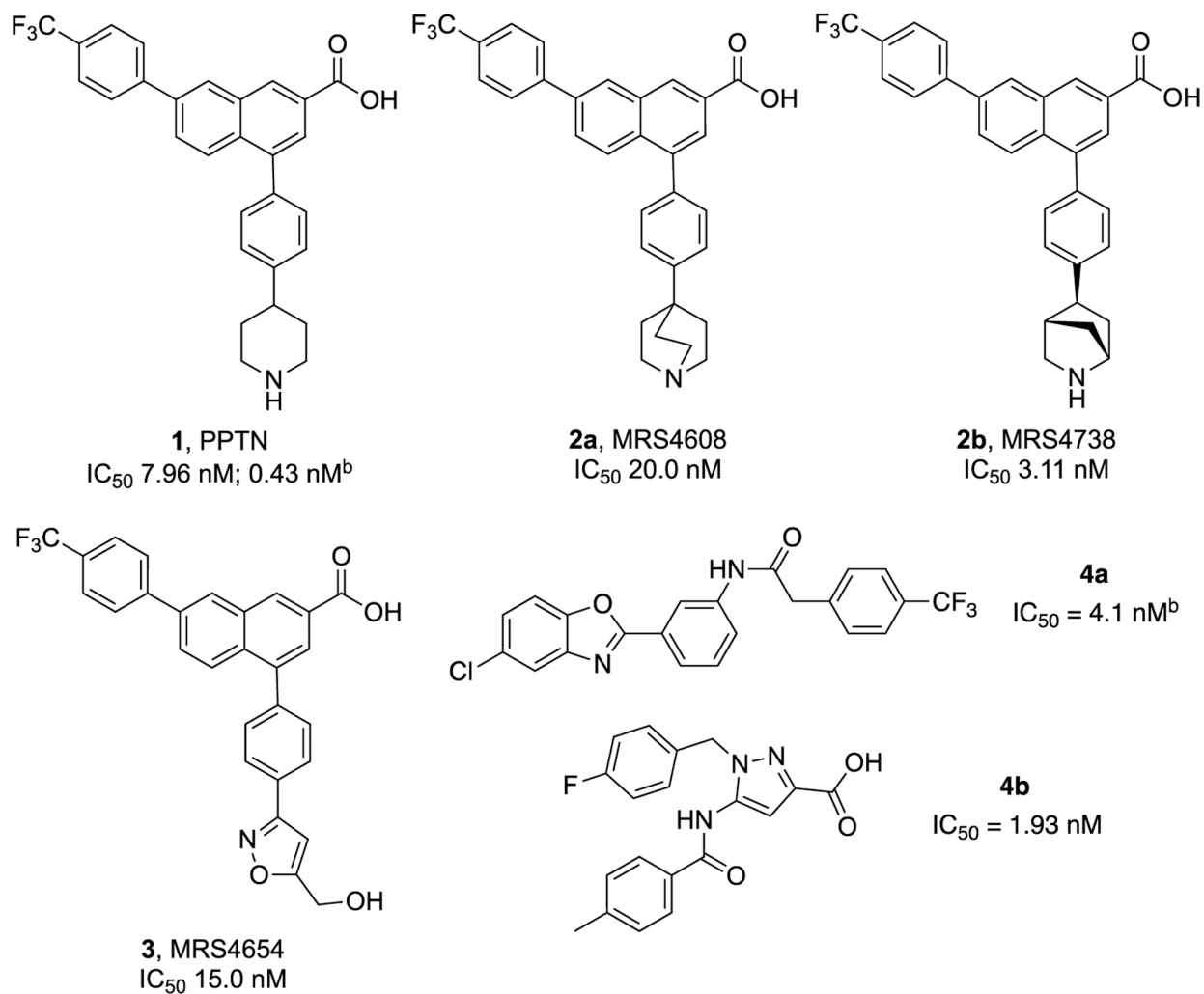


Chart 1.
Structures and Reported Potency^a of Representative P2Y₁₄R Antagonists, Derived from Lead Piperidine 1 (Including C-Bridged 2 and Uncharged 3 Bioisosteres) and Recently Reported 2-Phenyl-benzoxazole Acetamide 4a and 5-Amido-1*H*-pyrazole-3-carboxylic Acid 4b Derivatives^{20,21}

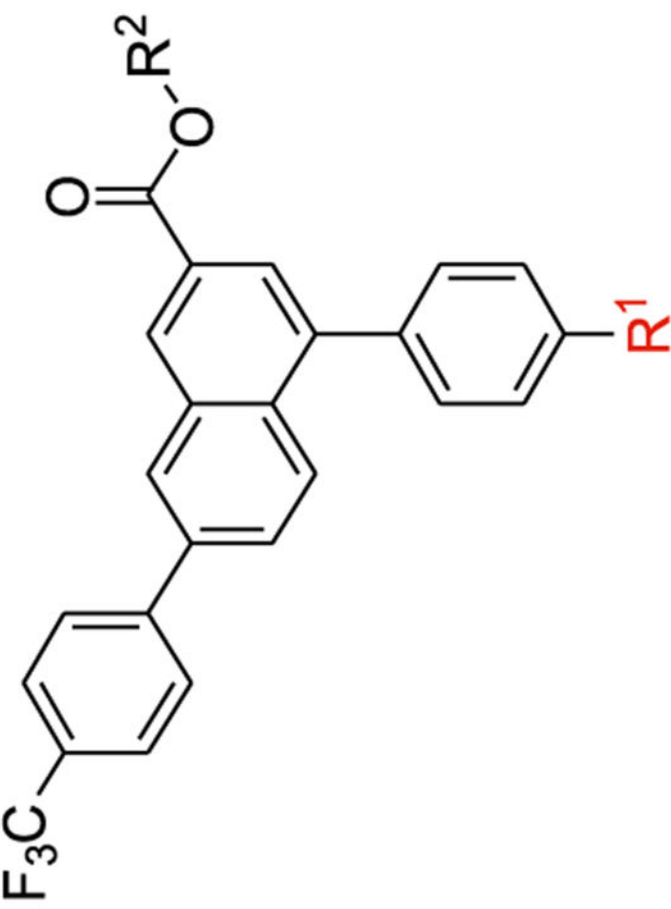
^bInhibitory activity in a cAMP assay.^{16,20a} IC_{50} in a fluorescent binding assay, unless noted.

Table 1.

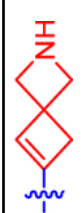


Structure and Affinity at hP2Y₁₄ R of Derivatives of Potent Antagonist 1^f

1, 2, 5 – 20, 49 – 51, 53, 57, 58, 62 – 64

No.	Structure, R ¹ =	IC ₅₀ (nM)	K _i (nM) ^d	Log D ₇₋₉ ^e	cLogD ^f	log([brain]); [blood] ^f
<i>4-membered rings</i>						
5		65.9±19.3	38.3	1.4±0.0	2.7	-0.869
6		46.6±7.1	27.1	1.9±0.0	3.1	-0.782



1, 2, 5 – 20, 49 – 51, 53, 57, 58, 62 – 64

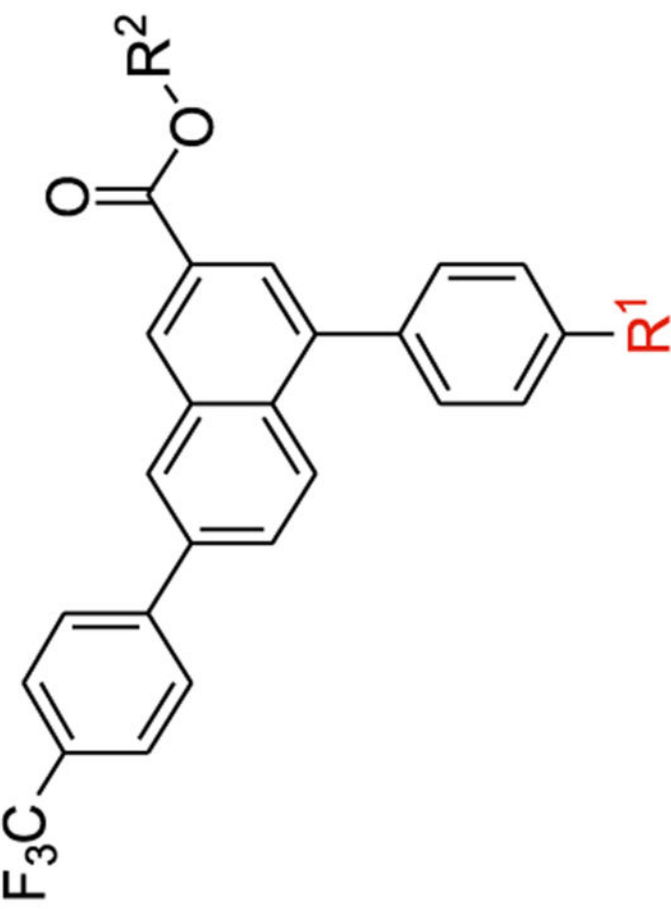
No.	Structure, R ¹ =	IC ₅₀ (nM)	K _i (nM) ^d	Log D ₇₋₄ ^e	cLogD ^f	log(brain): [blood] ^f
7		9.69±3.56	5.63	1.9±0.0	2.9	-0.717
8		20.8±5.6	12.1	0.81±0.0	2.2	-0.954
9 ^b		46.5±10.0	27.0	1.8±0.0	2.7	-0.835

Author Manuscript

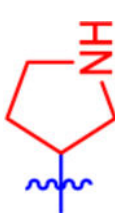
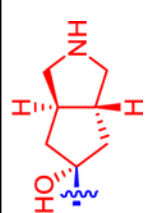
Author Manuscript

Author Manuscript

Author Manuscript



1, 2, 5 – 20, 49 – 51, 53, 57, 58, 62 – 64

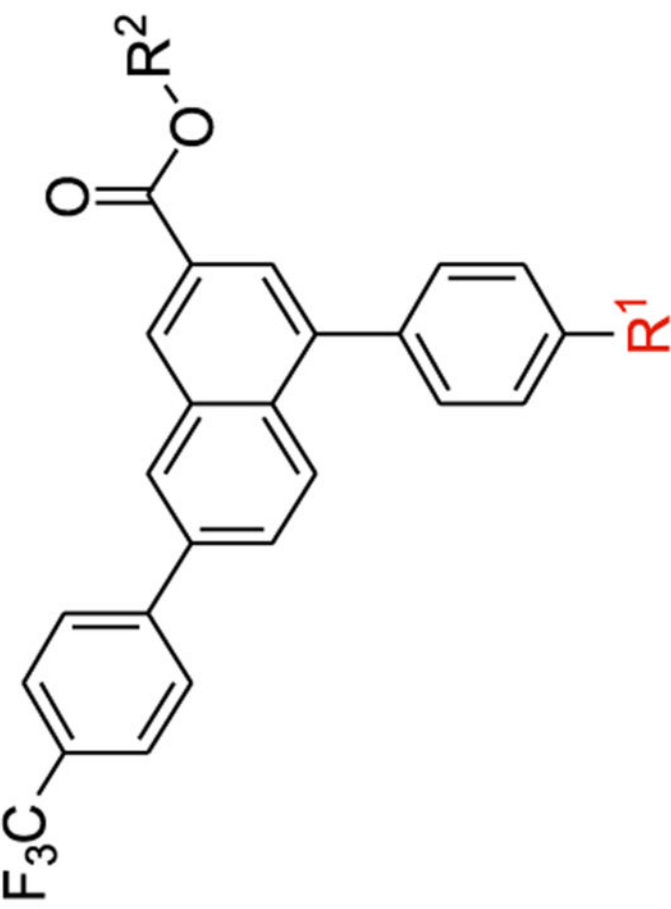
No.	Structure, R ¹ =	IC ₅₀ (nM)	K _i (nM) ^d	Log D _{7.4} ^e	cLogD ^f	log(brain): [blood] ^f
<i>5-membered rings</i>						
10 ^a		31.5±4.2	18.3	1.6±0.0	2.8	-0.869
11 ^a		9.48±1.66	5.51	1.1±0.0	2.4	-1.08

Author Manuscript

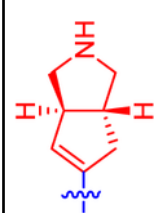
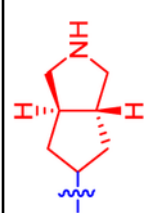
Author Manuscript

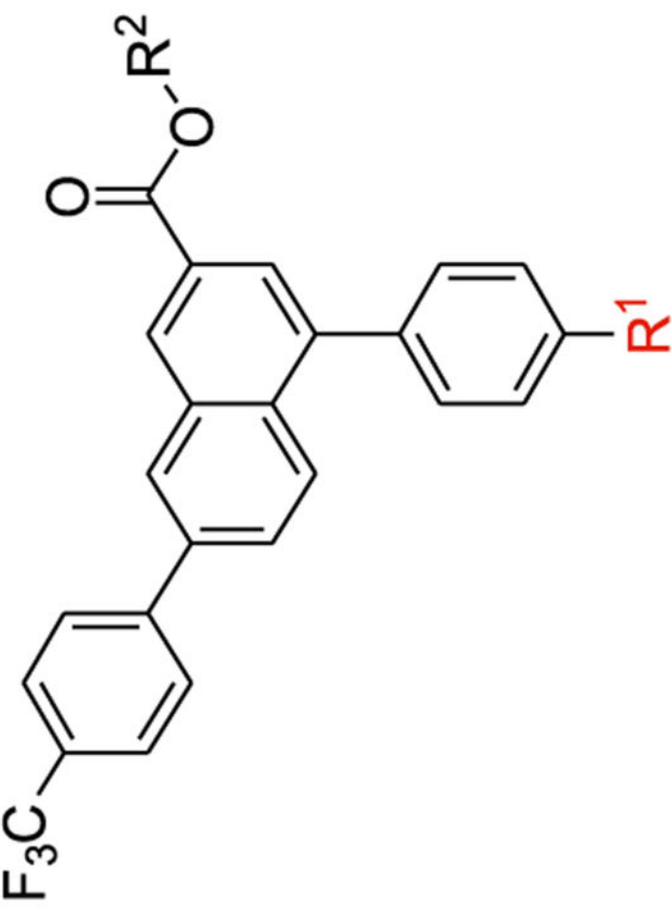
Author Manuscript

Author Manuscript

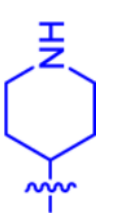



1, 2, 5 – 20, 49 – 51, 53, 57, 58, 62 – 64

No.	Structure, R ¹ =	IC ₅₀ (nM)	K _i (nM) ^d	Log D ₇₋₄ ^e	cLogD ^f	log(brain): [blood] ^f
12 ^a		16.6±3.2	9.65	2.2±0.0	3.1	-0.643
13 ^a		32.0±11.2	18.6	2.4±0.0	3.1	-0.877

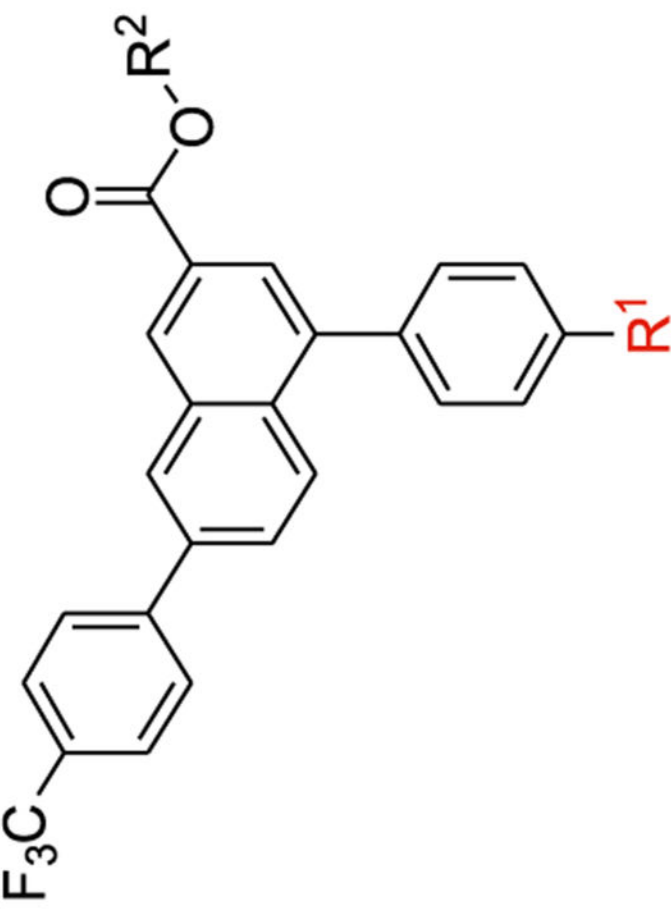
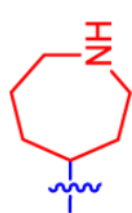


1, 2, 5 – 20, 49 – 51, 53, 57, 58, 62 – 64

No.	Structure, R ¹ =	IC ₅₀ (nM)	K _i (nM) ^d	Log D ₇₋₄ ^e	cLogD ^f	log(brain): [blood] ^f
<i>6-membered rings</i>						
1^c		7.96±0.35	4.63	1.7±0.0	2.9	-0.867
2a^c		20.0±4.4	11.6	4.2±0.9 ⁵	3.5	-0.577

No.	Structure, R ¹ =	IC ₅₀ (nM)	K _i (nM) ^d	Log D _{7.4} ^e	cLogD ^f	log(brain): [blood] ^f
2b ^c		3.11±0.62	1.81	1.9±0.1 ⁵	2.9	-0.874
14		524±104	305	2.8±0.0	3.1	-0.878

1, 2, 5 – 20, 49 – 51, 53, 57, 58, 62 – 64

No.	Structure, R ¹ =	IC ₅₀ (nM)	Ki (nM) ^d	Log D ₇₋₄ ^e	cLogD ^f	log([brain]: [blood]) ^f
15		5.92±0.55	3.44	1.2±0.0	2.4	-1.08
<i>7-membered rings</i>						
16 ^a		9.58±5.14	5.57	2.1±0.0	3.0	-0.861

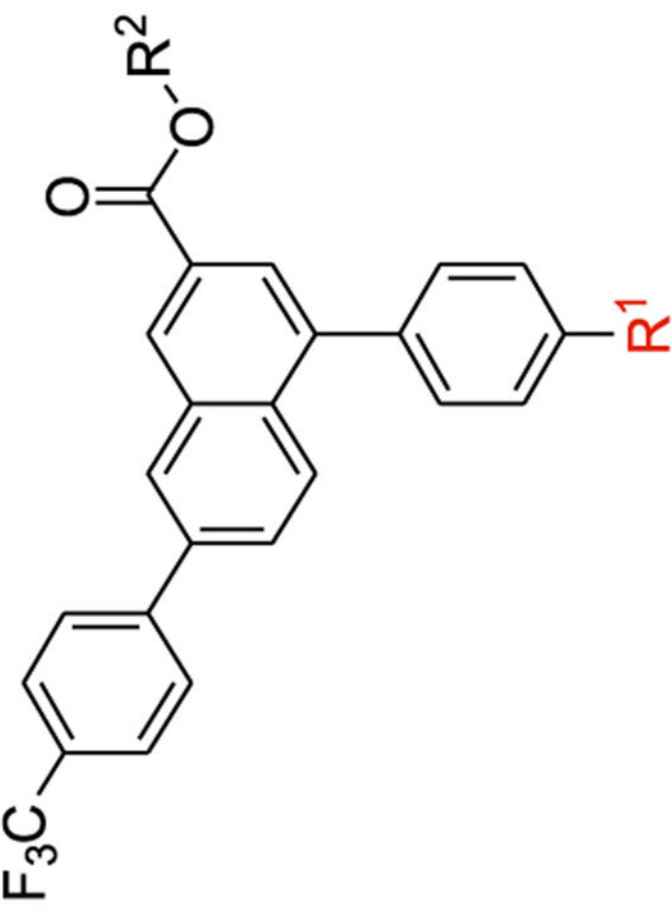
1, 2, 5 – 20, 49 – 51, 53, 57, 58, 62 – 64

Author Manuscript

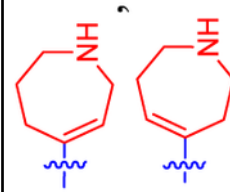
Author Manuscript

Author Manuscript

Author Manuscript



1, 2, 5 – 20, 49 – 51, 53, 57, 58, 62 – 64

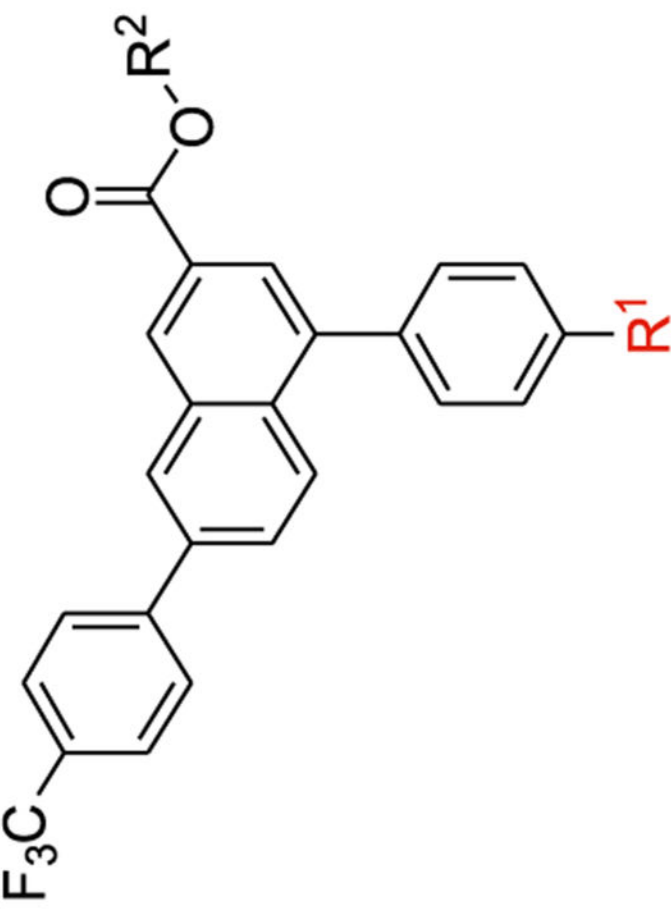
No.	Structure, R ¹ =	IC ₅₀ (nM)	K _i (nM) ^d	Log D ₇₋₄ ^e	cLogD ^f	log(brain): [blood] ^f
17 ^b		11.9±3.6	6.92	2.2±0.0	2.9	-0.612
<i>8-membered rings</i>						

Author Manuscript

Author Manuscript

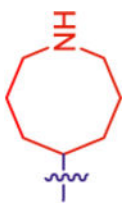
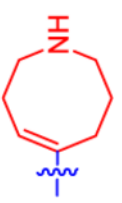
Author Manuscript

Author Manuscript



The chemical structure shows a naphthalene core. At the 1-position, there is a piperazine ring (highlighted in red) connected via its nitrogen atom to a benzene ring. This benzene ring has a trifluoromethyl group (F_3C) at the para position. At the 2-position of the naphthalene, there is another benzene ring. This benzene ring has an ester group ($-COOR^2$) at the para position and is connected at the other para position to a phenyl ring. This phenyl ring has an R^1 group at the para position.

1, 2, 5 – 20, 49 – 51, 53, 57, 58, 62 – 64

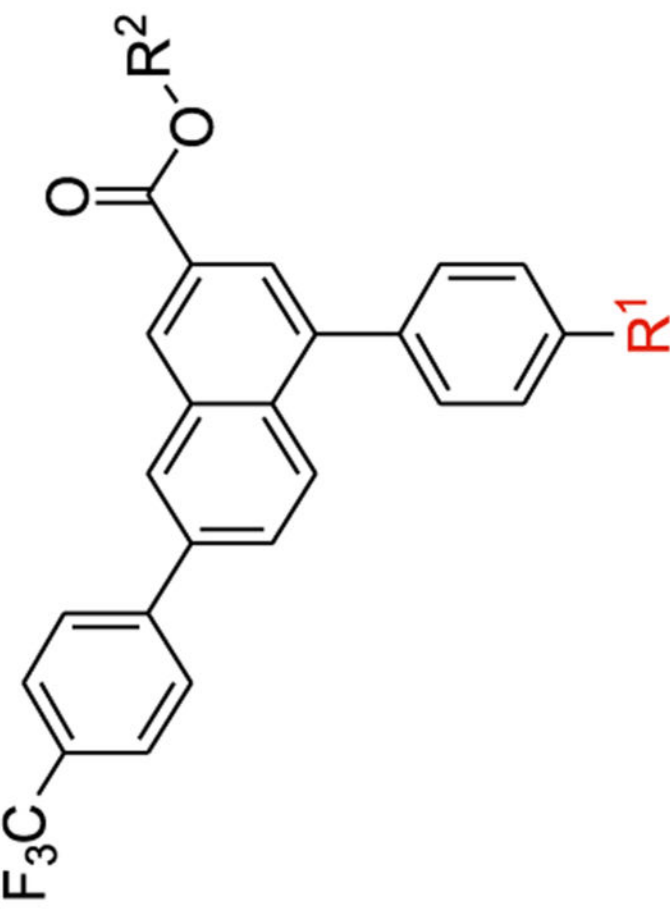
No.	Structure, $R^1 =$	IC ₅₀ (nM)	K _i (nM) ^d	Log D _{7.4} ^e	cLogD ^f	log(brain): [blood] ^f
18		18.5±4.8	10.8	2.5±0.0	3.1	-0.854
19		5 8.4± 16.4	34.0	2.9±0.0	3.0	-0.616

Author Manuscript

Author Manuscript

Author Manuscript

Author Manuscript

No.	Structure, R ¹ =	IC ₅₀ (nM)	K _i (nM) ^d	Log D ₇₋₄ ^e	cLogD ^f	log(brain): [blood] ^f
20		1780±440	1030	ND	2.2	-1.06
<i>prodrug derivatives of 1 and 1S</i>						

1, 2, 5 – 20, 49 – 51, 53, 57, 58, 62 – 64

Author Manuscript

Author Manuscript

Author Manuscript

Author Manuscript

1, 2, 5 – 20, 49 – 51, 53, 57, 58, 62 – 64

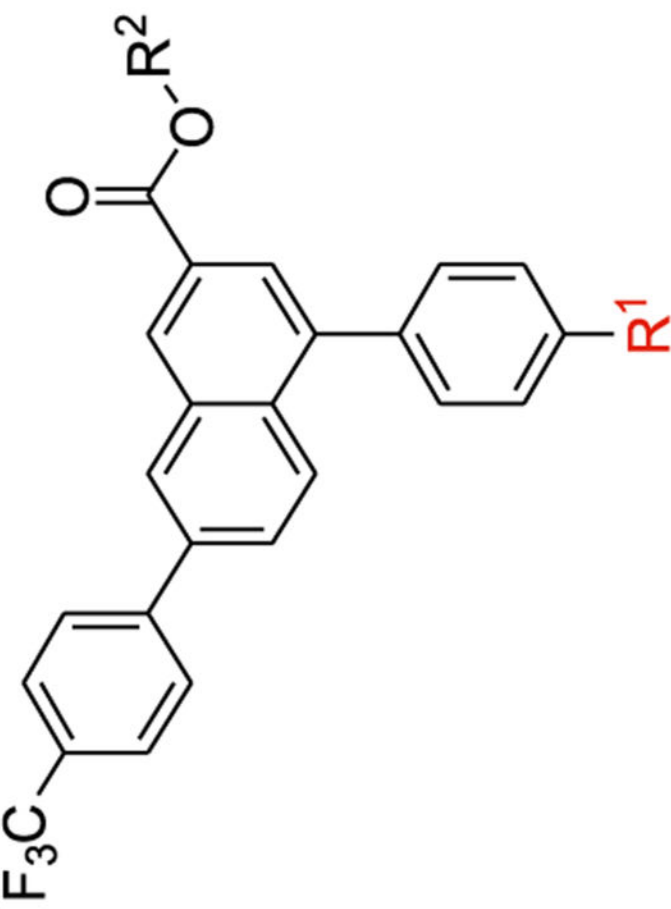
No.	Structure, R ¹ =	IC ₅₀ (nM)	K _i (nM) ^d	Log D ₇₋₄ ^e	cLogD ^f	log(brain): [blood] ^f
49	 R ² = $\text{CH}_2\text{CON}(\text{CH}_3)_2$	4810±1160	2800	ND	3.3	0.291
50	 R ² = $\text{CH}_2\text{CON}(\text{CH}_3)_2$	ND	ND	ND	5.4	-0.953

Author Manuscript


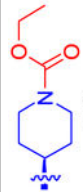
Author Manuscript

Author Manuscript

Author Manuscript



1, 2, 5 – 20, 49 – 51, 53, 57, 58, 62 – 64

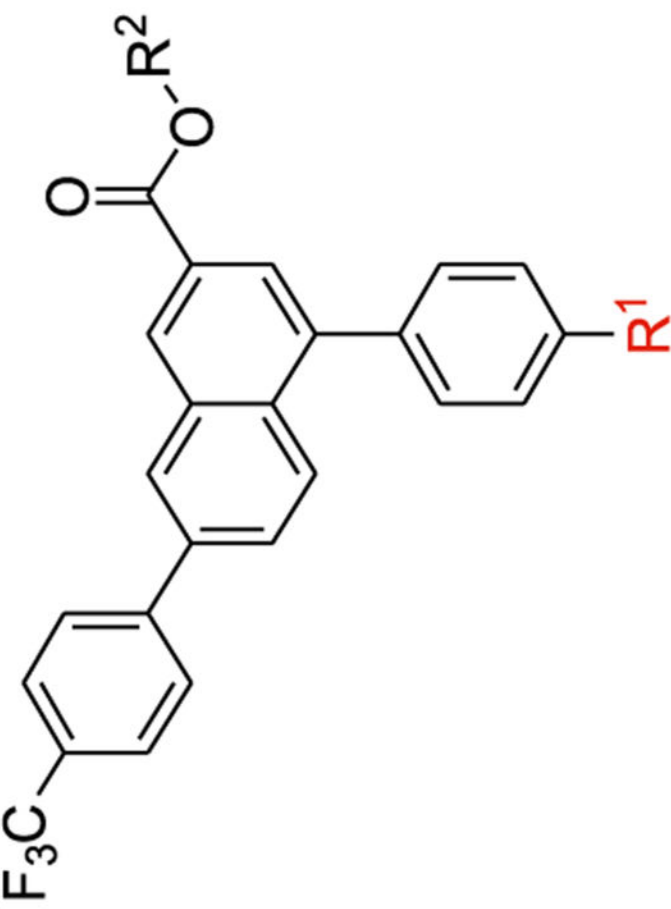
No.	Structure, R ¹ =	IC ₅₀ (nM)	K _i (nM) ^d	Log D _{7.4} ^e	cLogD ^f	log(brain): [blood] ^f
51		81.6±4.9	47.4	ND	3.3	-1.24
62	 R ² = <u>CH₂CON(CH₃)₂</u>	ND	ND	ND	6.4	-0.595

Author Manuscript



Author Manuscript

Author Manuscript

Author Manuscript



1, 2, 5 – 20, 49 – 51, 53, 57, 58, 62 – 64

No.	Structure, R ¹ =	IC ₅₀ (nM)	K _i (nM) ^d	Log D ₇₋₄ ^e	cLogD ^f	log(brain): [blood] ^f
63 ^c	 R ² = $\text{CH}_2\text{CON}(\text{CH}_3)_2$	ND	ND	ND	4.0	0.502
64 ^c	 R ² = $\text{CH}_2\text{CON}(\text{CH}_3)_2$	ND	ND	ND	6.5	-0.664

1, 2, 5 – 20, 49 – 51, 53, 57, 58, 62 – 64

No.	Structure, R ¹ =	IC ₅₀ (nM)	K _i (nM) ^d	Log D ₇₋₄ ^e	cLogD ^f	log([brain]: [blood]) ^f
<i>fluorescent derivative 53 and precursors</i>						
53	See Figure 1	25,900 ^h	9240 ^h	ND	3.6	-1.46
57	See Scheme S2	424±82	247	ND	4.3	-1.06
58	See Scheme S2	116±43 ^g	67.4	ND	3.7	-1.08

^aRacemate.^bMixture.^cFrom Wen et al., 2022 and Jung et al, 2020.^{5,17}^dCalculated from IC₅₀ values by dividing by 1.72 (see Figure S1, Supporting Information).

Author Manuscript

Author Manuscript

Author Manuscript

Author Manuscript

^eDistribution coefficient $\text{Log } D_{7.4}$ calculated from high-performance liquid chromatography (HPLC) retention factors k of ligands using the calibration curve of $\text{Log } D_{7.4}$ vs k generated from five standards with reported $\text{log } D_{7.4}$. (HPLC column: Agilent Eclipse XDB-C18 (4.6 mm \times 250 mm, 5 μm); Mobile phase: A: acetonitrile, B: 10 mM TEAA, 10%–100% A in 20 min; Flow rate: 1 mL/min).

^f $\text{cLog } D$ and blood–brain barrier (BBB) ratio calculated using the StarDrop program (v. 7.3.2, <https://www.optibrium.com/stardrop-installers>).²⁵

^gFluorescent binding IC_{50} value for long-chain amino derivative **58** was reported previously as 133 ± 13 nM.²⁶

^h $n = 1$.

ⁱThe affinity was determined using a whole-cell fluorescent binding assay (fluorescent tracer **52**); $R^2 = \text{H}$, and $n = 3\text{--}4$, unless noted. The piperidine moiety of **1** is shown in blue, while the various bridging groups, added functional groups, and other aliphatic (hetero)cyclic rings are shown in red. ND, not determined.

Table 2.Affinity of Selected Antagonists at the mP2Y₁₄R, Including Published Data on 1 and 2^{5,17}

compound	IC ₅₀ (nM)	IC ₅₀ ratio (mouse/human)
1	21.6 ± 7.0	2.71
2a	21.4 ± 7.9	1.07
2b	33.9 ± 4.6	10.9
7	15.9 ± 6.0	1.64
11	6.78 ± 1.58	0.715
12	5.57 ± 1.51	0.336
15	4.80 ± 0.70	0.811
16	25.7 ± 4.6	2.68
18	11.6 ± 0.9	0.627

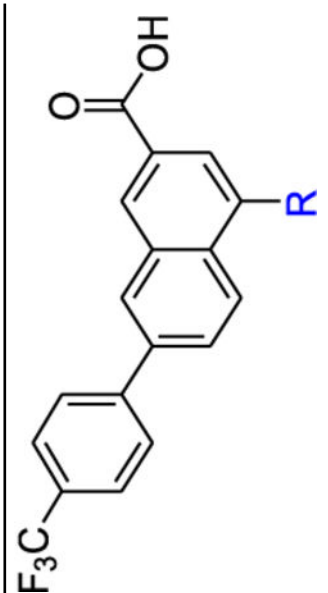

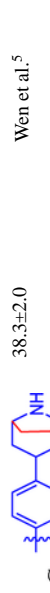

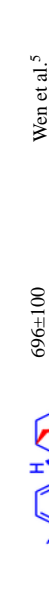
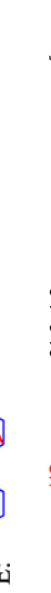
Author Manuscript

Author Manuscript

Author Manuscript

Author Manuscript

Previously Published Structures with Piperidine Ring Variation Showing the Effect on P2Y₁₄R Binding Affinity Associated with an α -Hydroxyl Substituent

R =	IC ₅₀ (P2Y ₁₄ R), nM ^a	Reference
	2.2 ^b	Belley et al. ¹⁵
	6.3 ^b	Belley et al. ¹⁵
	38.3±2.0	Wen et al. ⁵
	117±38	Wen et al. ⁵
	696±100	Wen et al. ⁵
	21.3±1.2	Wen et al. ⁵

^aHuman P2Y₁₄R, unless noted.

^bNonhuman primate (chimpanzee) P2Y₁₄R.

Table 4.

In Vitro ADMET Values for P2Y₁₄ R Antagonist 15 in This Study, Compared to Reference Antagonist 2b^a

test	2b ^b	15
simulated intestinal fluid (% remaining at 120 min)	99.1	93.3
simulated gastric fluid (% remaining at 120 min)	100 ^a	69.8
CYP1A2 (IC ₅₀ , μ M)	>30	>30
CYP2C9 (IC ₅₀ , μ M)	>30	>30
CYP2C19 (IC ₅₀ , μ M)	>30	>30
CYP2D6 (IC ₅₀ , μ M)	>30	>30
CYP3A4 (IC ₅₀ , μ M)	>30	>30
plasma stability (3 species) ^c (% remaining at 120 min)	82.8 (r); 100 (m)	81.3 (r); 100 (m); 91.1 (h)
microsomal stability (<i>t</i> _{1/2} , min)	243 (m), 91.0 (r), 280 (h)	355 (m), 342 (r), >400 (h)
hERG, IC50 (μ M)	>30	>30
hepG2 (human hepatoma) cell toxicity, IC50 (μ M) ^a	11.0	32.6 \pm 5.0
plasma protein binding (3 species, % bound)	99.76 (m), 99.79 (r), 87.98 (h)	99.86 (m), 99.48 (r), 99.30 (h)
solubility, (μ g/mL)	1.90 (pH 7.4) ^d	7.1 \pm 0.4 (pH 4.0), 1.4 \pm 0.1 (pH = 7.4) ^e

^aProcedures are described in Jung et al.¹⁷ hERG inhibition was measured using a fluorescent dye binding method (Supporting Information).

^bData determined in Wen et al.⁵

^cSpecies tested for plasma stability were human, rat, and mouse; species as indicated for microsomal stability.

^dMean \pm standard deviation (SD), pION method, determined by Jai Research Foundation (JRF) India of JRF Global (Gujarat, India).

^eMean \pm SD, pION method, determined at NIH.